

교 과 목 414.519 강의록

수 치 선 박 유 체 역 학

- 보 텍 스 방 법 -

**COMPUTATIONAL MARINE HYDRODYNAMICS**

**-VORTEX METHODS-**

2019년 6월 27일

Suh, Jung - Chun

서 정 천

Seoul National Univ., Dept. NAOE

서울대학교 공과대학 조선해양공학과

# 4

## POTENTIAL BASED METHODS

---

<b>4.1 Introduction</b> . . . . .	<b>154</b>
<b>4.2 Discretization of a Body Surface</b> . . . . .	<b>156</b>
4.2.1 Evaluation of the integrals for a line element . . . . .	157
<b>4.3 Trailing Wake Sheet Behind a Lifting Body</b> . . . . .	<b>159</b>
4.3.1 Boundary condtions . . . . .	159
4.3.2 Vortex distribution on wake sheet . . . . .	159
4.3.3 Doublet distribution (potential jump) on wake sheet . . . . .	161
4.3.4 Shedding vortex at trailing edge . . . . .	161
<b>4.4 Kutta Condition</b> . . . . .	<b>162</b>
4.4.1 Steady Kutta condition . . . . .	162
4.4.2 Unsteady Kutta condition. . . . .	163
<b>4.5 Analytic Solution for Elliptic Section in Steady Uniformly Sheared Flows</b> . . . . .	<b>165</b>
4.5.1 Conformal mapping . . . . .	165

4.5.2 Mapping coefficients . . . . .	167
4.5.3 Pressure, lift and moment . . . . .	168
4.5.4 Summarized results . . . . .	170
<b>4.6 Unsteady Lifting Flows for Two-Dimensional Hydrofoils . . . . .</b>	<b>172</b>
4.6.1 Equations of motion in a moving frame . . . . .	172
4.6.2 Representation of unsteady motion of a hydrofoil. . . . .	173
4.6.3 Representation of velocity field in a moving frame . . . . .	175
4.6.4 Formulation of boundary value problems for the disturbance potential. . . . .	175
4.6.5 Bernoulli-like equation in a moving frame . . . . .	177
4.6.6 Integral equation for disturbance potential. . . . .	179
4.6.7 Vortex model of shed wake sheet: Typical example . . . . .	181
4.6.8 Solution procedures. . . . .	184
4.6.9 Numerical results: Steady flow cases . . . . .	190
4.6.10 Numerical results: Unsteady flow cases . . . . .	192
<b>4.7 Formulation in Three-dimensions . . . . .</b>	<b>198</b>
4.7.1 Extension to 3-D wing . . . . .	198
4.7.2 Velocity components at a panel surface . . . . .	200
4.7.3 Non-lifting flow about an ellipsoid. . . . .	201
4.7.4 Lifting flow about a circular wing . . . . .	203

---

## 4.1 Introduction

We have provided the integral formulations for the flow analysis so far. Our first discussion will be an extended line concerning numerical analysis by panel methods. The key to this approach is the recognition that the surface integrals can be represented as a sum of integrals over elementary regions of the surface with no loss of generality.

We will require the elementary regions to sum to the real surface and make approximations in the calculations. In the limit as the number of elementary regions(or panels) tends to  $\infty$ , we expect this procedure to converge to the exact solution since it becomes the Riemann-sum definition of an integral. The utility of this analysis can be assessed by comparison with more exact procedures and with appropriate experimental data. In both analytic and numerical solutions, one seeks to solve a well-posed, or reasonable, problem.

For analytic problems this well-posed condition has been defined as that quality for which a bounded solution exists, the solution is unique, and the solution depends continuously on the data(in particular, small changes in the data produce small changes in the solution).

An extension of these concepts to numerical analysis is given by other researchers who point out that a well-posed computing problem(or algorithm a set of rules specifying the order and kind of arithmetic operations to be used on specific data) is existence, uniqueness in the sense that repeated runs produce the same result, and that the solution depends continuously on the data. In practice there is often more concern with existence than the other two properties of a well-posed problem.

We have a number of representations of the flow field that can be used to derive a solution for the specified boundary conditions. We need satisfy only the body boundary condition since the Laplace equation is already satisfied and the disturbances die off as  $\underline{x} \rightarrow \infty$ (so we have left only the body B.C. to meet).

One of the choices might be to use the results of the formulation in the previous chapter: In particular, we must consider our singularity distribution to be, in 3-D and in 2-D, respectively,

$$\frac{1}{2}\phi(\underline{x}_0) - \frac{1}{4\pi} \int_S \phi(\underline{y}) \frac{\underline{n}(\underline{y}) \cdot (\underline{x}_0 - \underline{y})}{|\underline{x}_0 - \underline{y}|^3} dS_y = -\frac{1}{4\pi} \int_S \underline{n} \cdot \nabla \phi(\underline{y}) \frac{1}{|\underline{x}_0 - \underline{y}|} dS_y \quad (4.1)$$

$$\frac{1}{2}\phi(\underline{x}_0) - \frac{1}{2\pi} \int_C \phi(\underline{y}) \frac{\underline{n}(\underline{y}) \cdot (\underline{x}_0 - \underline{y})}{|\underline{x}_0 - \underline{y}|^2} d\ell_y = -\frac{1}{2\pi} \int_C \underline{n} \cdot \nabla \phi(\underline{y}) \ln \frac{1}{|\underline{x}_0 - \underline{y}|} d\ell_y \quad (4.2)$$

where  $\underline{n}$  is directed from the body into the fluid field,  $\underline{n} \cdot \nabla \phi$  is known from the body B.C.:  $\underline{n} \cdot \underline{q} = 0 = \underline{n} \cdot (\underline{q}_\infty + \nabla \phi) \Rightarrow \underline{n} \cdot \nabla \phi = -\underline{n} \cdot \underline{q}_\infty$ .

On the RHS we set a known value for a given shape and onset flow and we would select a suitable discretization and approximation of the surface  $S_B$  and representation of the unknown  $\phi$ , say  $\phi$  is linear, bilinear, or even constant in each panel.

## 4.2 Discretization of a Body Surface

For 2-D flows, recall that our formulation would be

$$\boxed{\frac{1}{2}\phi(\underline{x}_0) = \frac{1}{2\pi} \int_C \left[ \phi(\underline{y}) \frac{\underline{n}(\underline{y}) \cdot (\underline{x}_0 - \underline{y})}{|\underline{x}_0 - \underline{y}|^2} - \underline{n} \cdot \nabla \phi(\underline{y}) \ln \frac{1}{|\underline{x}_0 - \underline{y}|} \right] d\ell_y} \quad (4.3)$$

The essence of the panel method approximation is to subdivide the surface into small elements. We can do this without loss of generality by specifying

$$\frac{1}{2}\phi(\underline{x}_0) = \frac{1}{2\pi} \sum_{j=1}^N \int_{C_j} \left[ \phi(\underline{y}) \frac{\underline{n}(\underline{y}) \cdot (\underline{x}_0 - \underline{y})}{|\underline{x}_0 - \underline{y}|^2} - \underline{n} \cdot \nabla \phi(\underline{y}) \ln \frac{1}{|\underline{x}_0 - \underline{y}|} \right] d\ell_y \quad (4.4)$$

where the  $C_j$  are a subdivision of the surface that will be sequentially ordered and one with some sort of formalism such that as  $N$  becomes large the maximum length of any  $C_j$  becomes arbitrarily fine. As  $N \rightarrow \infty$ , we know that one expression for the integral is the Riemann sum.

In using this representation, our interest is to approximate the integrals over  $C_j$  in some manner such that a relatively few number of elements is sufficient to provide an acceptable value for the integral. One of our choices is to consider a portion of the surface of the body. The element is defined to be bounded by the end points of the interval.

With this approach we would find a system of linear equations and solve them for  $\phi(\underline{y})$ . Once the values of  $\phi(\underline{y})$  are known, a differentiation of the values obtained would give the surface speed. We can call such a procedure a

low-order panel method.<sup>1</sup> Such procedures are reported to be cost effective, accurate, and simple to formulate. Note we solve for only the one scalar quantity even for 3-D flow (rather than 3 vector components)

The two-step process required to find the surface speed: that is, first, we must solve for the singularity distribution and then do another step (here taking the gradient) to find one of the quantities of great interest (the surface speed). Recall that once the surface speed is known we can use the Bernoulli equation to obtain the surface pressure and integrate the pressure to find loads.

#### 4.2.1 Evaluation of the integrals for a line element

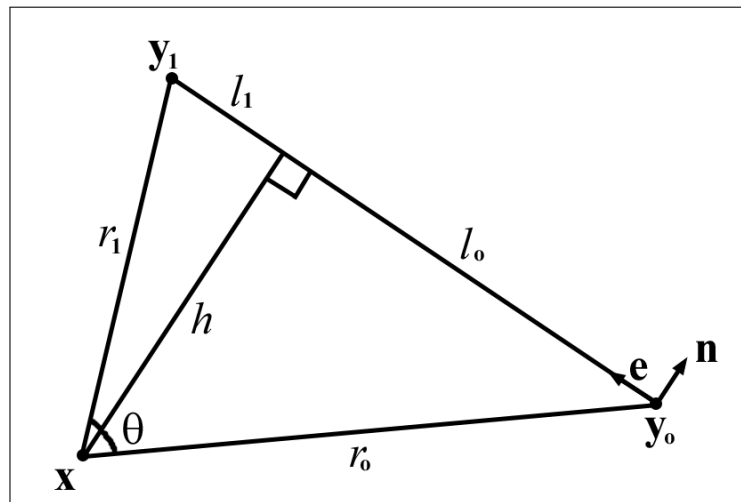


**Figure 4.1** Notation for evaluation of induction integrals on a line element.

The symbols shown in Figure (4.1) are defined as follows:

$$l = \left| \underline{y}_o - \underline{y}_1 \right|, \quad \underline{r}_o = \underline{y}_o - \underline{x}, \quad \underline{r}_1 = \underline{y}_1 - \underline{x}$$

$$l_o = -\underline{r}_o \cdot \underline{e}, \quad l_1 = \underline{r}_1 \cdot \underline{e}, \quad h = \underline{r}_o \cdot \underline{n} = \underline{r}_1 \cdot \underline{n}$$

$$\theta = \arctan \frac{l_o}{h} + \arctan \frac{l_1}{h} = \arctan \frac{2lh}{r_o^2 + r_1^2 - l^2}$$

Here,  $\underline{x}$  is the point to calculate the value and  $\underline{y}$  is defined on the body Panel as  $\underline{y} = \underline{y}_o + s \underline{e}$ .

<sup>1</sup>See Maskew, B. (1982), "Prediction of Subsonic Aerodynamic Characteristics of Panel Methods," *J. of Aircraft*, vol. 19, no. 2, pp. 157-163.

The Green function is written as

$$G = \frac{1}{2\pi} \ln r \quad (4.5)$$

$$\nabla G = \frac{1}{2\pi} \frac{\underline{r}}{r^2} = \frac{1}{2\pi} \frac{s \underline{e} + \underline{r}_o}{(s - l_o)^2 + h^2} \quad (4.6)$$

Then the associated integrals can be evaluated as follows:

(1) Calculation of  $\int \underline{n} \cdot \nabla G dl$

$$\begin{aligned} \int \underline{n} \cdot \nabla G dl &= \frac{1}{2\pi} \int_o^l \frac{\underline{n} \cdot (s \underline{e} + \underline{r}_o)}{(s - l_o)^2 + h^2} ds \\ &= \frac{h}{2\pi} \int_o^l \frac{ds}{(s - l_o)^2 + h^2} \\ &= \frac{1}{2\pi} \left( \arctan \frac{l_1}{h} + \arctan \frac{l_o}{h} \right) \\ &= \begin{cases} 0 & (\text{if } h = 0) \\ \frac{\theta}{2\pi} & (\text{if } h \neq 0) \end{cases} \end{aligned} \quad (4.7)$$

(2) Calculation of  $\int G dl$

$$\begin{aligned} \int G dl &= \frac{1}{2\pi} \frac{1}{2} \int_o^l \ln \left[ (s - l_o)^2 + h^2 \right] ds \\ &= \begin{cases} \frac{1}{2\pi} \left[ -l + \frac{1}{2} l_o \ln r_o^2 + \frac{1}{2} l_1 \ln r_1^2 \right] & (\text{if } h = 0) \\ \frac{1}{2\pi} \left[ -l + \frac{1}{2} l_o \ln r_o^2 + \frac{1}{2} l_1 \ln r_1^2 + h \theta \right] & (\text{if } h \neq 0) \end{cases} \end{aligned} \quad (4.8)$$

## 4.3 Trailing Wake Sheet Behind a Lifting Body

### 4.3.1 Boundary conditions

Assuming an inviscid fluid, the wake generated by time-varying flow around a lifting body appears as a discontinuity in the tangential flow velocity. In this case the infinitely thin wake sheet must be treated as a physical free boundary of the fluid region, or mathematically as a discontinuity of the domain. From a mathematical standpoint, a difference between two- and three-dimensional flow field disturbed by bodies is that the region occupied by fluid is double-connected in the two-dimensional case and single-connected in the three-dimensional case.<sup>2</sup> To ensure a unique solution, two boundary conditions are required; one is the kinematic boundary condition which states continuity of the velocity component normal to the vortex sheet:

$$(\underline{q}^+ - \underline{q}^-) \cdot \underline{n} = 0. \quad (4.9)$$

The other is the dynamic condition of no net stresses on the vortex sheet; i.e., the vortex sheet is a free surface. For inviscid fluid, this leads to the requirement that pressure be continuous across the sheet:

$$p^+ - p^- = 0. \quad (4.10)$$

### 4.3.2 Vortex distribution on wake sheet

A wake vortex sheet of vortex strength ( $\gamma$ ) is composed of vortices continuously produced at the T. E. according to the Kutta condition. The wake vortex sheet satisfying both the kinematic and the dynamic conditions, is deformed with time as flow conditions change. Let us denote the quantities in two regions separated by the wake sheet with the superscripts  $+$  and  $-$ . Then, from the kinematic condition the relative acceleration vectors on either side of the wake sheet in the

<sup>2</sup>See, e.g., Morino, L., Kaprielian, Z. and Sipcic, S. R. (1985), "Free Wake Analysis of Helicopter Rotors," *Vertica*, vol. 9, no. 2, pp. 127–140.

moving frame in the two regions can be written:

$$\underline{a}^+ = \frac{\partial \underline{q}^+}{\partial t} + \underline{q}^+ \cdot \nabla \underline{q}^+ = \frac{\partial \underline{q}^+}{\partial t} + \left( \underline{q}_m - \frac{\gamma}{2} \underline{t} \right) \cdot \nabla \underline{q}^+, \quad (4.11)$$

$$\underline{a}^- = \frac{\partial \underline{q}^-}{\partial t} + \underline{q}^- \cdot \nabla \underline{q}^- = \frac{\partial \underline{q}^-}{\partial t} + \left( \underline{q}_m + \frac{\gamma}{2} \underline{t} \right) \cdot \nabla \underline{q}^-, \quad (4.12)$$

where  $\underline{q}_m \equiv \frac{\underline{q}^+ + \underline{q}^-}{2}$  is the mean velocity on the wake sheet and the vortex strength  $\gamma$  is defined by  $\gamma \underline{t} = \underline{q}^- - \underline{q}^+$ , the tangential vector being taken as pointing downstream along the vortex sheet. From the Euler equations for the two regions, knowing that the additional acceleration terms resulting from taking the moving frame have the same value across the wake sheet, it follows that

$$(\underline{a}^+ - \underline{a}^-) = -\frac{1}{\rho}(\nabla p^+ - \nabla p^-), \quad (4.13)$$

where  $\rho$  is the (uniform) fluid density. The inner product of (4.13) with the sheet tangential vector gives

$$(\underline{a}^+ - \underline{a}^-) \cdot \underline{t} = 0. \quad (4.14)$$

This is because  $(\nabla p^+ - \nabla p^-) \cdot \underline{t}$  must be zero along the sheet by the dynamic condition of pressure continuity. Therefore, the governing equation for  $\gamma$  from (4.11), (4.12) and (4.14) becomes,

$$\frac{\partial(\gamma \underline{t})}{\partial t} \cdot \underline{t} + \left\{ \underline{q}_m \cdot \nabla(\gamma \underline{t}) \right\} \cdot \underline{t} + \gamma \left( \underline{t} \cdot \nabla \underline{q}_m \right) \cdot \underline{t} = 0, \quad (4.15)$$

or

$$\boxed{\frac{\partial \gamma}{\partial t} + \underline{q}_m \cdot \nabla \gamma + \gamma \underline{t} \cdot \frac{\partial \underline{q}_m}{\partial \ell} = 0,} \quad (4.16)$$

where  $\frac{\partial}{\partial \ell}$  denotes the differential in the tangential direction ( $\underline{t}$ ) along the sheet. The last term represents the effect of the local stretching of the sheet on the variation of the vortex strength with time.

### 4.3.3 Doublet distribution (potential jump) on wake sheet

A second alternate wake sheet singularity is that of doublets with strength corresponding to the jump in disturbance potential ( $\Delta\phi_v$ ). This distribution is also governed by the kinematic and dynamic conditions ((4.9) and (4.10)). The subscript  $v$  will be used to refer to values at the wake sheet.

If the pressure relation given by (4.74) is applied to the upper and the lower sides of the sheet, respectively, the following two equations are obtained:

$$\frac{p^+}{\rho} + \frac{\partial\phi^+}{\partial t} - \frac{1}{2}\underline{q}_F^2 + \frac{1}{2}\underline{q}^{+2} + \underline{q}_o \cdot \underline{q}_F = C(t), \quad (4.17)$$

$$\frac{p^-}{\rho} + \frac{\partial\phi^-}{\partial t} - \frac{1}{2}\underline{q}_F^2 + \frac{1}{2}\underline{q}^{-2} + \underline{q}_o \cdot \underline{q}_F = C(t). \quad (4.18)$$

Subtracting (4.18) from (4.17), and knowing that the other terms without a superscript have the same value on the both sides of the sheet under the assumption of zero thickness of the sheet, we have

$$\left( \frac{D(\Delta\phi_v)}{Dt} \right)_m = \left( \frac{D(\phi^+ - \phi^-)}{Dt} \right)_m = \boxed{\frac{\partial(\phi^+ - \phi^-)}{\partial t} + \underline{q}_m \cdot \nabla(\phi^+ - \phi^-) = 0}. \quad (4.19)$$

Here the kinematic and dynamic conditions have been used. Equation (4.19) implies that the fixed value of the jump in disturbance potential across the wake vortex sheet is convected with the mean velocity on the sheet. This statement is equivalent to Kelvin's circulation theorem describing the constancy of circulation round any closed material curve. The disturbance potential jump across the sheet corresponding to a doublet distribution with strength  $\mu(\underline{x}_v, t) (= \Delta\phi_v = \phi^+ - \phi^-)$  can be replaced by an equivalent vorticity distribution.

### 4.3.4 Shedding vortex at trailing edge

When including the influence of the wake sheet in the derivation of an analytic solution, the use of (4.19) for the doublet distribution might be easier in manipulation than that of (4.16) for the vorticity distribution on the sheet. The

reason is that we need an extra consideration of the sheet geometry caused by the third term of (4.16) representing the local stretching of the vortex sheet. Another advantage of the numerical implementation of (4.19) is that the value of the potential jump at the T. E. determined by the Kutta condition at each time step can be directly assigned to a fixed value on the wake sheet that just left the T. E.

Meanwhile the position vector  $\underline{x}_v(t)$  of a point of fixed  $\Delta\phi_v$  value on the shed-vortex sheet that left the T. E. at time  $t_o$  ( $t_o > 0$ ) is given by the non-linear relation:

$$\underline{x}_v(t) = \int_{t_o}^t \underline{q}_m(\underline{x}_v(\tau)) d\tau + \underline{x}_{TE}. \quad (4.20)$$

To calculate the mean velocity ( $\underline{q}_m$ ) in (4.19), the position of the wake sheet must be prescribed by using the integral form given by (4.20). There appears to be a non-linear coupled effect between the mean velocity and the position of the wake sheet.

One of the important features related to the wake sheet in unsteady flow about the foil is a time-varying bound circulation. Applying (4.19) as a point on the wake sheet approaches the T. E. becomes

$$\frac{d\Gamma_B}{dt} = -\underline{q}_m \cdot \underline{t} \Big|_{TE} \gamma_{TE}, \quad (4.21)$$

where we define the (disturbance) bound circulation by  $\Gamma_B = -(\phi^+ - \phi^-)|_{TE}$  (with positive taken as counterclockwise) and the shed vorticity at the T. E. by  $\gamma_{TE} \underline{t} = -\nabla(\phi^+ - \phi^-)_{TE}$ . Equation (4.21) is closely related to the unsteady Kutta condition as described in the next section.

## 4.4 Kutta Condition

### 4.4.1 Steady Kutta condition

The Kutta condition has been applied originally in the steady two-dimensional flow case for uniqueness of solution mathematically and for regular flow in the

vicinity of the T. E. physically. It eventually implies that the rear stagnation point is at the T. E. for a non-cusped sharp-edged foil in order to satisfy both the pressure-equality condition and the condition of finite velocity at the T. E.

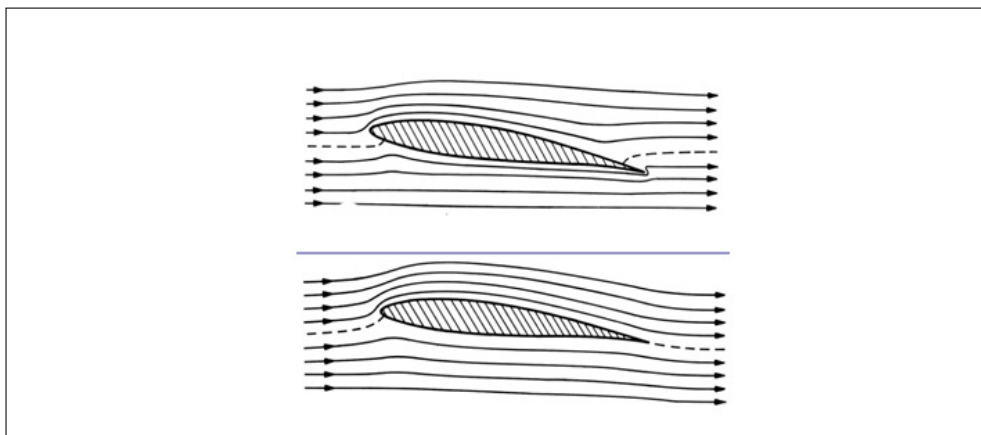


**Figure 4.2** Flow past a foil without circulation, and with a properly selected circulation so that a stagnation point is at T.E. From Newman (1977).

There are two commonly used types of the steady (and possibly unsteady) Kutta condition in a panel method. One type, say ‘wake-tangency type’, consists of selecting a point at a short distance out in the fluid along the wake sheet element attached to the T. E. with a given inclination angle and requiring the flow at that point to be tangent to that element.

The other type, say ‘pressure-equality type’, consists of requiring equal values of velocity at the control points on the two panel elements adjacent to the T. E. In some cases, significant variations in the overall circulation and local flow properties may result from different choices for the type and/or the location of the application point of the numerical Kutta condition.

#### 4.4.2 Unsteady Kutta condition

But if we applied this interpretation in unsteady flow (in which we have a shed vortex sheet trailing downstream and a time derivative term in the pressure relation), an unacceptable situation will occur; either infinite vortex strength ( $\gamma_{TE} = \infty$ ) or  $d\Gamma_B/dt = 0$  at the T. E. as is easily seen in (4.21), whereas shed vorticity ( $\gamma_{TE}$ ) as well as the mean velocity ( $\underline{q}_m$ ) at the T. E. should remain finite.

Unlike the steady two-dimensional flow cases, the two conditions of pressure equality and finite velocity can not be applied exactly at the T. E., unless one of the two conditions is sacrificed to save the other one. The reason is that there is inherently a velocity difference (shed-vortex strength) across the sharp T. E.

Following the concepts based on the pressure-equality condition and the finiteness of velocity, Mangler & Smith<sup>3</sup> have investigated the trailing-edge flow for steady three-dimensional lifting problems. The essential result is that the flow leaves the T. E. parallel to either the upper or lower surface depending on the sign of the vorticity in the sheet as it leaves the T. E. The possible orientation of the sheet is limited to be between the tangents of the foil surface at the T. E., otherwise an infinite velocity will occur. As an extension of Mangler and Smith's approach to the unsteady two-dimensional flow case, the so-called 'Maskell' trailing-edge flow is discussed by Basu & Hancock and Morino et al.<sup>4</sup>

There is no rigorous model of the unsteady Kutta condition for general unsteady motions unless the viscous effect is fully investigated. However it is considered acceptable to employ a numerical scheme by which a resulting solution should satisfy nearly the condition of finite velocities and the condition of zero loading in the neighborhood of the T. E. or at the T. E. The unsteady Kutta condition adopted possibly in the numerical method is

- (1) to introduce the wake sheet as a 'barrier' for the existence of a single-valued potential function in the fluid region about the foil,
- (2) to assume a parabolic form for potential values ( $\phi$ ) along the upper and lower foil surfaces so that the potential jump can be extrapolated to the T. E. as points on the foil surface approach the T. E. (the stagnation point can be located at either the upper or the lower trailing edge, depending on the sign of  $d\Gamma_B/dt$ ), and

<sup>3</sup>Mangler, K. W. and Smith, J. H. B. (1970), "Behaviour of the Vortex Sheet at the Trailing Edge of a Lifting Wing," *Aeronautical Journal of the Royal Aeronautical Society*, vol. 74, pp. 906–908.

<sup>4</sup>Basu, B. C. and Hancock, G. J. (1978), "The Unsteady Motion of a Two-Dimensional Aerofoil in Incompressible Inviscid Flow," *Journal of Fluid Mechanics*, vol. 87, pp. 159–178.

Morino, L., Kaprielian, Z. and Sipcic, S. R. (1985), "Free Wake Analysis of Helicopter Rotors," *Vertica*, vol. 9, no. 2, pp. 127–140.

(3) to select a point at a short-distance off the T. E. along a straight-line wake sheet element attached to the T. E. and require the flow at that point to be tangent to the sheet. This model requires an iteration procedure to determine the potential jump and the orientation of the straight-line wake sheet element at the T. E. The iteration process for the orientation of the straight-line element is similar to that of Basu & Hancock.<sup>5</sup> The difference in calculated global forces between the scheme using the ‘Maskell’ local behavior and the present scheme using the Basu & Hancock procedure for the orientation of the straight-line element is small to negligible (although not illustrated herein) except that if the former is used, the results against time is not smooth at a few time steps near instants at which the sign of the rate of the bound circulation changes. The numerical implementation of the Kutta condition will be described in Appendix A.

## 4.5 Analytic Solution for Elliptic Section in Steady Uniformly Sheared Flows

### 4.5.1 Conformal mapping

It is desirable to obtain some exact solutions for steady uniform shear-flow about specific profiles in order to confirm the validity of numerical methods used in the present work.<sup>6</sup> For uniformly sheared onset flow with an inviscid incompressible fluid in 2-D, the disturbance potential exists and its governing equation is the Laplace equation.

A typical solution method is the extension of the classical conformal mapping technique where the foil in the physical plane is mapped into a circle in the complex plane. The known flow about the circle is then transformed to that about the physical shape. Among many available conformal transformations,

---

<sup>5</sup>Basu, B. C. and Hancock, G. J. (1978), “The Unsteady Motion of a Two-Dimensional Aerofoil in Incompressible Inviscid Flow,” *Journal of Fluid Mechanics*, vol. 87, pp. 159–178.

<sup>6</sup>The details are referred to Suh (1990).

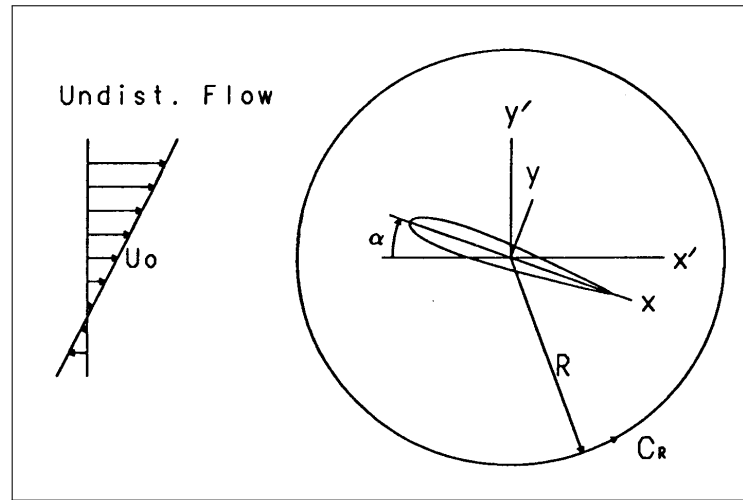


**Figure 4.3** Foil configuration for steady uniformly sheared onset flow.  $U_o$  is a reference velocity of undisturbed flow at  $y' = 0$  parallel to  $x'$ -axis.  $C_R$  is a control surface of a circle with a radius  $R$ .

the Moriya conformal mapping function suggested by Moriya <sup>7</sup> might be used for the purpose of validating the numerical methods developed against analytical results.

The conformal transformation is specified generally as

$$z = x + iy = C_{-1} \frac{\zeta}{a} + C_o + \sum_{n=1}^{\infty} C_n \frac{a^n}{\zeta^n}, \quad (4.22)$$

where  $z = x + iy$  is the complex coordinate of a point in the physical plane ( $z$ -plane),  $\zeta = \xi + i\eta$  is the complex coordinate in the circle plane ( $\zeta$ -plane),  $a$  is a characteristic length dimension (taken as the radius of a circle that is set to 1 for non-dimensionalization), and  $C_n = A_n + iB_n$  are complex mapping constants. Specially for an ellipse with thickness-chordlength ratio  $\tau$ , all  $C_n$ 's are zero except  $A_{-1} = (1 + \tau)/4$ ,  $A_1 = (1 - \tau)/4$ .

Then the  $x$ -coordinates of the surface points can be expressed as  $x_s(\theta) = \frac{c}{2} \cos \theta$  where  $\theta$  is polar coordinates in the circle plane where  $c$  is chordlength. The  $y$ -

<sup>7</sup>Moriya, T. (1941), "On the Aerodynamic Theory of an Arbitrary Wing Section," *Journal of the Society of Aeronautical Sciences*, vol. 8, no. 78, pp. 1054–1060, English version: *Selected Scientific and Technical Papers*, University of Tokyo, 1959, pp. 48–59.

coordinates of the points on the upper surface are defined as:

$$y_s(\theta) = \frac{c}{2} \tau \sin \theta \quad (4.23)$$

### 4.5.2 Mapping coefficients

Now, we assume the complex disturbance potential  $F_1(\zeta)$  as, satisfying the Laplace equation and the far-field behavior:

$$F_1(\zeta) = \phi_1 + i \psi_1 = -i \frac{\Gamma_B}{2\pi} \ln \zeta + c_1 \frac{1}{\zeta} + c_2 \frac{1}{\zeta^2} + \dots, \quad (4.24)$$

where  $\phi_1$  is the disturbance potential and  $\psi_1$  is the disturbance stream function. Here the disturbance bound circulation  $\Gamma_B$  (with positive as counterclockwise) and the complex coefficients  $c_n (= \alpha_n + i \beta_n)$  are to be determined by using the kinematic body boundary condition and the Kutta condition at the T. E.

The kinematic boundary condition on the circle in the  $\zeta$ -plane becomes

$$\frac{1}{r} \frac{\partial \psi_1}{\partial \theta} \Big|_{r=1} = - \left( \underline{q}_\infty \cdot \underline{n} \left| \frac{dz}{d\zeta} \right| \right) \Big|_{\zeta=e^{i\theta}}, \quad (4.25)$$

where the undisturbed (sheared onset) velocity  $\underline{q}_\infty$  in the  $z$ -plane is given by:

$$\underline{q}_\infty = U_o \left\{ 1 + \frac{K}{c} (y \cos \alpha - x \sin \alpha) \right\} \underline{i}' \quad (4.26)$$

where  $K$  is the gradient of shear inflow velocity. From (4.25), the coefficients  $\alpha_n$  and  $\beta_n$  (non-dimensionalized by the chordlength  $c$ , the radius of the circle  $a$  and the reference speed  $U_o$ ) are determined (calculation is lengthy but straightforward):

$$\begin{aligned} \alpha_1 &= (A_{-1} - A_1) \cos \alpha, \\ \beta_1 &= (A_{-1} + A_1) \sin \alpha, \\ \alpha_2 &= -A_2 \cos \alpha - \frac{K}{4} (A_{-1}^2 - A_1^2) \sin 2\alpha, \\ \beta_2 &= A_2 \sin \alpha + \frac{K}{4} \left[ (A_{-1} - A_1)^2 \cos^2 \alpha - (A_{-1} + A_1)^2 \sin^2 \alpha \right] \end{aligned} \quad (4.27)$$

where the coefficients with  $n$  greater than 2 in Eq. (4.24) are zero.

Now, to find  $\Gamma_B$ , a stagnation point should be imposed at the T. E. (as the Kutta condition):

$$\left( -\frac{\partial\psi_1}{\partial r} + \underline{q}_o \cdot \underline{t} \left| \frac{dz}{d\zeta} \right| \right) \Big|_{\substack{r=1 \\ \theta=0}} = 0. \quad (4.28)$$

Inserting (4.27) for the coefficients  $\alpha_n$  and  $\beta_n$  into (4.28) and arranging for  $\Gamma_B$ , we find

$$\frac{\Gamma_B}{2\pi U_o c} = - \left[ \sum_{n=1}^2 n \beta_n + (A_{-1} - A_1) \left( 1 - \frac{K}{2} \sin \alpha \right) \sin \alpha \right]. \quad (4.29)$$

The total surface  $q_s$  in the direction of increasing  $\theta$  is

$$\begin{aligned} \frac{q_s(\theta)}{U_o} = & \left[ \{1 + K(y \cos \alpha - x \sin \alpha)\} \left( \frac{dx}{d\theta} \cos \alpha + \frac{dy}{d\theta} \sin \alpha \right) \right. \\ & \left. + \left\{ \frac{\Gamma_B}{2\pi} + \sum_{n=1}^2 n(-\alpha_n \sin n\theta + \beta_n \cos n\theta) \right\} \right] / \sqrt{\left( \frac{dx}{d\theta} \right)^2 + \left( \frac{dy}{d\theta} \right)^2} \Big|_{r=1} \end{aligned} \quad (4.30)$$

Here  $\frac{dx}{d\theta} \Big|_{r=1}$  and  $\frac{dy}{d\theta} \Big|_{r=1}$  are the  $x$ - and  $y$ -component of the surface tangential vector in the direction of increasing  $\theta$ , respectively:

$$\frac{dx}{d\theta} \Big|_{r=1} = -(A_{-1} + A_1) \sin \theta, \quad \frac{dy}{d\theta} \Big|_{r=1} = (A_{-1} - A_1) \cos \theta. \quad (4.31)$$

### 4.5.3 Pressure, lift and moment

A Bernoulli equation for two-dimensional steady flow with constant vorticity is given by,<sup>8</sup>

$$\frac{p}{\rho} + \frac{q^2}{2} + \omega_o \psi = \text{constant}. \quad (4.32)$$

<sup>8</sup>See Yih, C.-S. (1977), *Fluid Mechanics*, McGraw-Hill, p. 70.

where  $\psi$  denotes stream function value that depends on streamlines concerned. Then the pressure coefficient along the profile is,

$$C_p \left( \equiv \frac{p - p_\infty}{\frac{1}{2} \rho U_o^2} \right) = (1 + 2KC_\psi) - \frac{q_s^2}{U_o^2}, \quad (4.33)$$

or within an additive constant,

$$C_p = 1 - \frac{q_s^2}{U_o^2}. \quad (4.34)$$

The force components  $F_x$  and  $F_y$  (in the  $x$ - and  $y$ - direction of the coordinate system fixed on the foil) and the moment acting on the foil (about the origin) are expressed as an integral of the pressure and velocity distribution on the enclosing circle from the conservation theorem for momentum and angular momentum:<sup>9</sup>

$$\begin{aligned} F_x &= - \int_{C_R} p dy - \int_{C_R} \rho q_x (q_x dy - q_y dx), \\ F_y &= \int_{C_R} p dx - \int_{C_R} \rho q_y (q_x dy - q_y dx), \\ M_o &= \int_{C_R} p (x dx + y dy) - \int_{C_R} \rho (x q_y - y q_x) (q_x dy - q_y dx), \end{aligned} \quad (4.35)$$

where  $q_x$  and  $q_y$  are, respectively, the  $x$ - and  $y$ - component of the total velocity on the contour  $C_R$  with a sufficiently large radius ( $R$ ) in the physical plane. (See Figure 4.3 ).

First the inversion of the mapping function is given by

$$\zeta = \frac{z}{A_{-1}} - \frac{A_o}{A_{-1}} - \frac{A_1}{z} - \frac{A_o A_1 + A_2^2}{z^2} + \dots \quad (4.36)$$

Then (4.24) for the complex (disturbed) velocity potential is inverted as a power

<sup>9</sup>See, for details, Tsien, H.-S. (1943), "Symmetrical Joukowski airfoils in shear flow," *Quarterly of Applied Mathematics*, vol. 1, pp. 130–148.

series of  $z$ :

$$\begin{aligned}
F_1(z) &= -i \frac{\Gamma_B}{2\pi} \ln \frac{z}{A_{-1}} + \left\{ i \frac{\Gamma_B}{2\pi} A_o + (\alpha_1 + i \beta_1) A_{-1} \right\} \frac{1}{z} \\
&+ \left\{ i \frac{\Gamma_B}{2\pi} \left( A_{-1} A_1 + \frac{1}{2} A_o^2 \right) + A_{-1} A_o (\alpha_1 + i \beta_1) + A_{-1}^2 (\alpha_2 + i \beta_2) \right\} \frac{1}{z^2} \\
&+ \dots .
\end{aligned} \tag{4.37}$$

Then, the disturbance velocity  $\underline{u}$  can be expressed as

$$u_x - i u_y = \frac{dF_1}{d\zeta} \frac{d\zeta}{dz} \Big|_{\zeta=re^{i\theta}} \tag{4.38}$$

Now using (4.36) and (4.37) together with (4.27), (4.32) and (4.38) for the velocity components and the pressure, we find the lift and the moment coefficients (about the mid-chord point):

$$C_L = 4\pi(a_o - K b_1), \tag{4.39}$$

$$C_{M_o} = -4\pi(a_1 + K b_2), \tag{4.40}$$

where

$$a_o = -\frac{\Gamma_B}{2\pi}, \tag{4.41}$$

$$a_1 = A_{-1} \beta_1 \cos \alpha - A_{-1} \alpha_1 \sin \alpha, \tag{4.42}$$

$$b_1 = -A_{-1} \beta_1 \sin \alpha - A_{-1} \alpha_1 \cos \alpha, \tag{4.43}$$

$$b_2 = -A_{-1}^2 \alpha_2 \cos 2\alpha - \left( A_{-1} A_1 \frac{\Gamma_B}{2\pi} + A_{-1}^2 \beta_2 \right) \sin 2\alpha. \tag{4.44}$$

Here it is noted that  $\Gamma_B$ ,  $A_n$ ,  $\alpha_n$  and  $\beta_n$  have been non-dimensionalized by  $U_o$ ,  $c$  and  $a$ .

#### 4.5.4 Summarized results

For an ellipse with the thickness ratio  $\tau$ , the quantities  $q_s$ ,  $C_p$ ,  $C_L$  and  $C_{M_o}$  can be expressed simply in terms of  $K$ ,  $\alpha$ ,  $\tau$  as:

$$\frac{q_s}{U_o} = \frac{(e_o + e_1 \sin \theta + e_2 \cos \theta + e_3 \sin 2\theta + e_4 \cos 2\theta)}{\sqrt{\sin^2 \theta + \tau^2 \cos^2 \theta}}, \quad (4.45)$$

$$C_p = \left\{ 1 + \frac{K^2}{8} (\tau^2 \cos^2 \alpha + \sin^2 \alpha) \right\} - \frac{q_s^2}{U_o^2}, \quad (4.46)$$

$$C_L = \pi \left\{ 2(1 + \tau) \sin \alpha + K\tau \left( \tau \cos^2 \alpha - \sin^2 \alpha + \frac{1}{2} \right) \right\}, \quad (4.47)$$

$$C_{M_o} = \frac{\pi}{64} (1 - \tau^2) \sin 2\alpha \{ 16 + 8K(1 + \tau) \sin \alpha + K^2(1 + 3\tau) (\tau \cos^2 \alpha - \sin^2 \alpha) \}, \quad (4.48)$$

where

$$e_o = -(1 + \tau) \left\{ \sin \alpha + \frac{K}{4} (\tau \cos^2 \alpha - \sin^2 \alpha) \right\}, \quad (4.49)$$

$$e_1 = -(1 + \tau) \cos \alpha, \quad (4.50)$$

$$e_2 = (1 + \tau) \sin \alpha, \quad (4.51)$$

$$e_3 = \frac{K}{4} (1 + \tau)^2 \cos \alpha \sin \alpha, \quad (4.52)$$

$$e_4 = \frac{K}{4} (1 + \tau) (\tau \cos^2 \alpha - \sin^2 \alpha). \quad (4.53)$$

For uniform onset flows, we can simply set  $K = 0$  in the above results to have the solution. The exact value of the surface speed is given, for a general angle of attack  $\alpha$ , by

$$\frac{q_s}{U} = (1 + \tau) \left[ \frac{\sin \theta \cos \alpha + (1 - \cos \theta) \sin \alpha}{\sqrt{\sin^2 \theta + \tau^2 \cos^2 \theta}} \right] \quad (4.54)$$

The lift coefficient is  $C_L = 2\pi(1 + \tau) \sin \alpha$ .

## 4.6 Unsteady Lifting Flows for Two-Dimensional Hydrofoils

### 4.6.1 Equations of motion in a moving frame

Let  $\underline{q}(x, y, z, t)$  describe the flow field in a moving coordinate system that is in motion relative to a space fixed system  $x', y', z'$ . In general, the relations between coordinates, velocities, and accelerations are those of Eqs. (1.208–1.211);

$$\underline{x}' = \underline{x} + \underline{R} \quad (4.55)$$

$$\underline{q}' = \underline{q} + \underline{\dot{R}} + \underline{\Omega} \times \underline{x} \quad (4.56)$$

$$\frac{d'\underline{q}}{dt} = \frac{d\underline{q}}{dt} + 2\underline{\Omega} \times \underline{q} + \underline{\dot{\Omega}} \times \underline{x} + \underline{\Omega} \times (\underline{\Omega} \times \underline{x}) + \underline{\ddot{R}} \quad (4.57)$$

Thus the left-hand side of Eq. (4.57) must be augmented by addition of four new terms, in general, in order to constitute a differential equation for  $\underline{q}(x, y, z, t)$ .

On the other hand, space derivatives such as grad, div, and curl are unaffected in form by the transformation of axes. The only change in such terms therefore arise from the process of carrying out these operations on quantities, such as  $\underline{q}$ , which have additional terms. There are no such terms in the scalar quantity  $p$ ; hence Eq. (4.57) are altered only by addition of the four new left-hand terms mentioned.

Before writing down the new equation of motion, let us consider the equation of continuity. Consider the term  $\nabla' \cdot \underline{q}'$ , and let  $\nabla \cdot$  denote the divergence operator in the moving system:

$$\nabla' \cdot \underline{q}' = \nabla \cdot \underline{q}' = \nabla \cdot (\underline{q} + \underline{\dot{R}} + \underline{\Omega} \times \underline{x}) = \nabla \cdot \underline{q} \quad (4.58)$$

because the divergences of the last two terms are zero (see Eq. (1.67)). The physical meaning of this result should be clear to the reader.

Thus the equations for the general case of fluid motion described in a moving coordinate system are

$$\frac{D\rho}{Dt} + \rho \nabla \cdot \underline{q} = 0 \quad (4.59)$$

and

$$\frac{D\underline{q}}{Dt} + 2\underline{\Omega} \times \underline{q} + \dot{\underline{\Omega}} \times \underline{x} + \underline{\Omega} \times (\underline{\Omega} \times \underline{x}) + \ddot{\underline{R}} = -\frac{1}{\rho} \nabla p + \underline{F}_B + \nu \nabla^2 \underline{q} \quad (4.60)$$

#### 4.6.2 Representation of unsteady motion of a hydrofoil

A two-dimensional foil of finite thickness and/or camber with a fixed mean angle of attack in uniform onset flow of an incompressible inviscid fluid is assumed to undergo combined unsteady periodic motions (and/or sudden start-up motion).

Since the first effort is concerned with the disturbance velocity field, this section now gives the formulation of the boundary value problem for the unknown disturbance velocity potential.

In most unsteady problems it is convenient to adopt a moving reference frame fixed relative to the body and then to define the flow field relative to the moving body, for which the geometric definition of a rigid body is time-independent.

Figure 4.4 represents a relative configuration of a body in the inertial and moving frames with appropriate notations to be used for the formulation of the boundary value problem. Note that the prime notation ( $\prime$ ) refers to the quantities expressed in the inertial frame. Here the origin ( $O$ ) of the moving frame is located at the mid-chord point of the foil and the  $x$ -axis is taken as an extension of the chordline.

The vectors  $\underline{\rho}_F(t)$  and  $\underline{x}_p (= x_p \underline{i} + y_p \underline{j})$  are the position vector of a reference point (herein taken as the pivot point of a pitching motion) measured in the inertial and the moving frame, respectively.

The vector  $\underline{\Omega}(t) (= \Omega(t) \underline{k})$  for two-dimensional motion, with positive taken as counterclockwise) is the angular velocity of the moving frame about the reference point. Then  $\underline{q}_F (= \dot{\underline{\rho}}_F(t) + \underline{\Omega}(t) \times (\underline{x} - \underline{x}_p))$  represents the velocity (observed in the inertial frame) at a field point ( $\underline{x}_p$ ) in the moving frame due to its translational and angular motions relative to the inertial frame. We shall call  $\underline{q}_F$



### 4.6.3 Representation of velocity field in a moving frame

It is important to note that the vorticity is not the same in the two systems. Using the primes as before, we see that, according to Eq. (1.68),

$$\nabla' \times \underline{q}' = \nabla \times \underline{q}' = \nabla \times (\underline{q} + \dot{\underline{R}} + \underline{\Omega} \times \underline{x}) = \nabla \times \underline{q} + 2 \underline{\Omega} \quad (4.63)$$

We find the physical meaning of this result. An important case is one of flow that is irrotational but is viewed in a rotating coordinate system; it appears to be rotational. The case of a rotating propeller frame is typical.

The total velocity, observed in the inertial frame fixed in space is made up of two parts:

$$\underline{q}'_T(\underline{x}', t) = \underline{q}'_o(\underline{x}') + \underline{u}'(\underline{x}', t), \quad (4.64)$$

where  $\underline{q}'_o(\underline{x}')$  is an onset velocity field that satisfies the continuity equation itself (a steady potential flow when measured in the inertial frame) and  $\underline{u}'(\underline{x}', t)$  is the disturbance velocity component to be determined herein.

In the moving frame the total velocity is the sum of the frame velocity ( $\underline{q}_F$ ) and the fluid velocity ( $\underline{q}$ ) measured by an observer in the moving frame:

$$\underline{q}_T(\underline{x}, t) = \underline{q}_F(\underline{x}, t) + \underline{q}(\underline{x}, t), \quad (4.65)$$

where  $\underline{x}$  and  $\underline{q}$  are measured relative to the moving frame.

Equating the two different expressions of Eqs. (4.64) and (4.65), the relative velocity ( $\underline{q}$ ) is expressed by

$$\boxed{\underline{q}(\underline{x}, t) = \underline{q}'_o(\underline{x}, t) - \underline{q}_F(\underline{x}, t) + \underline{u}(\underline{x}, t)} \quad (4.66)$$

### 4.6.4 Formulation of boundary value problems for the disturbance potential.

According to the representation of the foil motion and the velocity field as outlined in the previous subsection, the flow characteristics about a foil can be

determined by solving the boundary value problem for the disturbance velocity ( $\underline{u}$ ) relative to the known undisturbed velocity field ( $\underline{q}_o - \underline{q}_F$ ).

Now, let the foil be assumed to undergo unsteady (not necessarily sinusoidal) rigid motions in a uniform, unbounded onset flow field of an inviscid incompressible fluid, with any static effects due to the gravity ignored.

Then the continuity equation applied to the total velocity ( $\underline{q}'_T$ ) in the inertial reference frame becomes (since the differential operators with respect to space coordinates have the same value)

$$\nabla' \cdot \underline{q}'_T = \nabla \cdot (\underline{q}_F + \underline{q}) = 0. \quad (4.67)$$

Since  $\nabla \cdot \underline{q}_F = \nabla \cdot (\dot{\underline{\rho}}_F + \underline{\Omega} \times (\underline{x} - \underline{x}_p)) = 0$  and  $\nabla \cdot \underline{q}_o = 0$ , the continuity equation applied to the relative velocity ( $\underline{q}$ ) in the moving frame is expressed by

$$\nabla \cdot \underline{q} = \nabla \cdot (\underline{u} - \underline{q}_F + \underline{q}_o) = 0. \quad (4.68)$$

Thus the continuity equation in the moving frame for the disturbance velocity reduces to  $\nabla \cdot \underline{u} = 0$ , which implies that working in a moving frame does not affect the expression of the continuity equation.

For uniqueness, there remain conditions to be imposed on the boundary of the fluid region. The kinematic body boundary condition (tangency condition or no-penetration condition) on the rigid body surface (represented by  $B(\underline{x})$ ) can be expressed in terms of the disturbance velocity ( $\underline{u}$ ) observed in the moving frame:

$$\underline{u} \cdot \underline{n} \left( \equiv \frac{\partial \phi}{\partial n} \right) = -(\underline{q}_o - \underline{q}_F) \cdot \underline{n} \quad (4.69)$$

In the presence of an elastic deformation (which is not considered in the present work), the normal component of the local velocity of deformation is added on the right-hand side of the above equation.

In addition, the far-field condition (i.e.,  $\underline{u} \rightarrow 0$  far away from the body), the Kutta condition at the T. E., and the kinematic and the dynamic conditions on the shed-vortex sheet (represented by  $W(\underline{x}, t)$ ) should be satisfied for the existence of a unique disturbance velocity ( $\underline{u}$ ) or velocity potential ( $\phi$ ) for any

lifting problem.

The fluid potential ( $\phi$ ) is determined by solving the boundary value problem at discrete time steps in a step-by-step fashion, or at arbitrary time, either analytically or numerically. Once the potential is known, the disturbance velocity field is obtained by taking the gradient of the disturbance potential ( $\phi$ ). The velocity field is then obtained by adding the undisturbed velocity field and the disturbance velocity as in (4.66). Finally the surface pressure distributions, and the forces and the moments acting on the foil section can be computed, respectively, by using a Bernoulli-like equation (which is described in the following subsection) and integrating the pressure on the body surface.

#### 4.6.5 Bernoulli-like equation in a moving frame

The Euler equation in an inertial reference frame may be put in the form, neglecting external body force potential terms:

$$\frac{\partial' \underline{q}_T}{\partial t} - \underline{q}_T \times (\nabla' \times \underline{q}_T) = -\nabla' \left( \frac{p}{\rho} + \frac{1}{2} \underline{q}_T^2 \right). \quad (4.70)$$

Knowing that the gradient operators have the same form in either inertial or non-inertial reference frame, we reduce this equation to

$$\frac{\partial'(\underline{q}_o + \underline{u})}{\partial t} - (\underline{q} + \underline{q}_F) \times (\nabla \times (\underline{q}_o + \underline{u})) = -\nabla \left( \frac{p}{\rho} + \frac{1}{2} (\underline{q} + \underline{q}_F)^2 \right). \quad (4.71)$$

Because the onset velocity distribution  $\underline{q}_o$  is usually a function of only the space position in the inertial reference frame (i.e.,  $\partial \underline{q}'_o(\underline{x})/\partial t = 0$ ) and the disturbance velocity ( $\underline{u}$ ) is irrotational (i.e.  $\underline{u} = \nabla \phi$ ), Eq. (4.71) becomes

$$\nabla \left( \frac{\partial' \phi}{\partial t} \right) - (\underline{q} + \underline{q}_F) \times (\nabla \times \underline{q}_o) + \nabla \left( \frac{p}{\rho} + \frac{1}{2} (\underline{q} + \underline{q}_F)^2 \right) = 0. \quad (4.72)$$

We can convert the operator  $\left(\frac{\partial'}{\partial t}\right)$  in the inertial frame into  $\left(\frac{\partial}{\partial t} - \underline{q}_F \cdot \nabla\right)$  in the moving frame.<sup>10</sup> This indicates that the rate of change of a quantity (say  $\phi$ ) at a point fixed in the space-fixed frame is measured by an observer in the moving frame. We can then write Eq. (4.72) as

$$\nabla \left( \frac{p}{\rho} + \frac{\partial \phi}{\partial t} + \frac{1}{2} \underline{q}^2 - \frac{1}{2} \underline{q}_F^2 + \underline{q}_o \cdot \underline{q}_F \right) - (\underline{q} + \underline{q}_F) \times (\nabla \times \underline{q}_o) = 0. \quad (4.73)$$

For irrotational onset flow, the pressure equation can be written as

$$\frac{p}{\rho} = -\frac{\partial \phi}{\partial t} + \frac{1}{2} \underline{q}_F^2 - \frac{1}{2} \underline{q}^2 - \underline{q}_o \cdot \underline{q}_F + C(t). \quad (4.74)$$

For the case of marine propellers, we may take  $C(t) = \frac{p_\infty}{\rho} + \frac{1}{2} V_s^2$  and  $\underline{q}_F = \underline{\Omega} \times \underline{x} = -2\pi n r \underline{e}_\theta$  for right-hand rotation, where  $V_s$  is ship speed and  $\underline{e}_\theta$  is the unit vector of the propeller-rotation direction.

The resulting expression for the unsteady pressure coefficient ( $C_p$ ) non-dimensionalized by a reference speed  $U_o$  (which is typically taken as an undisturbed main uniform velocity or the moving speed of a body) is

$$C_p \left( \equiv \frac{p - p_\infty}{\frac{1}{2} \rho U_o^2} \right) = \frac{\rho H_o - p_\infty}{\frac{1}{2} \rho U_o^2} - \frac{2}{U_o^2} \frac{\partial \phi}{\partial t} + \frac{\underline{q}_F^2}{U_o^2} - \frac{\underline{q}^2}{U_o^2} - \frac{2 \underline{q}_o \cdot \underline{q}_F}{U_o^2}, \quad (4.75)$$

where  $H_o$  is a Bernoulli constant representing total energy-head at the reference point far away from the body, and  $p_\infty$  the reference pressure in the inertial frame far away from the body. To within an additive constant, it becomes

$$C_p = -\frac{2}{U_o^2} \frac{\partial \phi}{\partial t} + \frac{\underline{q}_F^2}{U_o^2} - \frac{\underline{q}^2}{U_o^2} - \frac{2 \underline{q}_o \cdot \underline{q}_F}{U_o^2}. \quad (4.76)$$

<sup>10</sup>See Milne-Thomson, L. M. (1968), *Theoretical Hydrodynamics*, fifth ed., Macmillan, London, p. 89, and Kochin, N. E., Kibel, I. A. and Roze, N. V. (1964), *Theoretical Hydrodynamics*, Interscience Publishers Inc., p. 116.

### 4.6.6 Integral equation for disturbance potential

We will consider two-dimensional lifting flow field for a hydrofoil for our specific examples and general formulation. The problem of defining the velocity field has been reduced to solving the Laplace equation for the disturbance (perturbation) potential ( $\phi$ );

$$\nabla^2 \phi = 0 \text{ in the fluid region,} \quad (4.77)$$

being subject to the no-penetration condition on the body surface;

$$\underline{u} \cdot \underline{n} \left( \equiv \frac{\partial \phi}{\partial n} \right) = - \left( \underline{q}_o - \underline{q}_F \right) \cdot \underline{n} \text{ on } B(\underline{x}) \quad (4.78)$$

the Kutta condition at the T. E. given by (A.10), the combined kinematic and dynamic conditions on the shed-vortex sheet;

$$\frac{\partial(\phi^+ - \phi^-)}{\partial t} + \underline{q}_m \cdot \nabla(\phi^+ - \phi^-) = 0 \text{ on } W(\underline{x}) \quad (4.79)$$

and a far-field decay condition;

$$\phi \rightarrow \text{constant as } r \rightarrow \infty. \quad (4.80)$$

The disturbance velocity potential ( $\phi$ ) which satisfies the Laplace equation in the fluid region with a ‘barrier’ representing the wake sheet can be represented in the form of an integral equation based on Green’s scalar (second) identity:

$$\begin{aligned} \phi(\underline{x}, t) &= \frac{1}{2\pi} \int_B \left( \frac{\partial \phi(\underline{y}, t)}{\partial n} \ln |\underline{x} - \underline{y}| + \phi(\underline{y}, t) \frac{\underline{n}(\underline{y}) \cdot (\underline{x} - \underline{y})}{|\underline{x} - \underline{y}|^2} \right) d\ell_y \\ &+ \frac{1}{2\pi} \int_W \Delta \phi_v \frac{\underline{n} \cdot (\underline{x} - \underline{y})}{|\underline{x} - \underline{y}|^2} d\ell_y. \end{aligned} \quad (4.81)$$

Here the range of integration of the position vector of the source point ( $\underline{y}$ ) representing the dummy variable of the integrals is the body surface contour  $B(\underline{x})$  and the wake sheet  $W(\underline{x}_v, t)$ . The contribution of the integration along the contour of infinite radius enclosing the body goes to a constant as the radius

of the circuit goes to infinity because the net flux of volume of fluid becomes zero for a closed rigid body.<sup>11</sup>

The unit normal vectors ( $\underline{n}$ ) point outward from the body surface and upward at the wake sheet, and  $\Delta\phi_v$  is the jump in the disturbance potential ( $\phi^+ - \phi^-$ ) across the wake sheet of zero thickness. The superscripts + and - indicate the limit on the upper and the lower side, respectively, of the sheet. This integral representation is more efficient in computation time than direct solution of the Euler equation (say, by a finite difference scheme) (since only the surface values of the physical quantities are concerned).

Evaluating the limit of the integral as a field point ( $\underline{x}$ ) approaches a point on the body surface ( $\underline{x}_o$ ) gives the integral equation for the unknown distribution of the disturbance potential ( $\phi$ ):<sup>12</sup>

$$\begin{aligned} \phi(\underline{x}_o, t) &= \frac{1}{2\pi} \oint_B \left( \frac{\partial\phi}{\partial n} \ln |\underline{x}_o - \underline{y}| + \phi \frac{\underline{n} \cdot (\underline{x}_o - \underline{y})}{|\underline{x}_o - \underline{y}|^2} \right) d\ell_y \\ &+ \frac{1}{2} \phi(\underline{x}_o, t) + \frac{1}{2\pi} \int_W \Delta\phi_v \frac{\underline{n} \cdot (\underline{x}_o - \underline{y})}{|\underline{x}_o - \underline{y}|^2} d\ell_y, \end{aligned} \quad (4.82)$$

where the first integral denotes a Cauchy principal value integral. Also, inserting (4.78) for  $\partial\phi/\partial n$  (equivalent source strength) into (4.82) gives a two-dimensional Fredholm integral equation of the second kind for the disturbance potential ( $\phi$ ):

$$\begin{aligned} \frac{1}{2} \phi(\underline{x}_o, t) - \frac{1}{2\pi} \oint_B \phi \frac{\underline{n} \cdot (\underline{x}_o - \underline{y})}{|\underline{x}_o - \underline{y}|^2} d\ell_y &= \\ \frac{1}{2\pi} \oint_B \left( \underline{q}_F - \underline{q}_o \right) \cdot \underline{n} \ln |\underline{x}_o - \underline{y}| d\ell_y &+ \frac{1}{2\pi} \int_W \Delta\phi_v \frac{\underline{n} \cdot (\underline{x}_o - \underline{y})}{|\underline{x}_o - \underline{y}|^2} d\ell_y. \end{aligned} \quad (4.83)$$

If the shape of the wake sheet and the potential jump ( $\Delta\phi_v$ ) are specified

<sup>11</sup>It may be chosen arbitrarily without failure of uniqueness of the velocity field. In the present work this constant is taken to be zero as the far-field value along the circuit far away from the body. See also Batchelor, G. K. (1967), *An Introduction to Fluid Dynamics*, Cambridge University Press, Cambridge, p. 126.

<sup>12</sup>For the limiting forms for integral expressions of surface distribution of various singularities (source, vortex and doublet), see Brockett, T. E., Kim, M.-H. and Park, J.-H. (1989), "Limiting Forms for Surface Singularity Distributions When the Field Point is on the Surface," *Journal of Engineering Mathematics*, vol. 23, pp. 53–79.

from the Kutta condition at the T. E. (Eq. (A.10)) and the combined kinematic and dynamic conditions on the shed-vortex sheet ((4.79)), the surface potential distribution can be obtained by solving this integral equation. The velocity field is obtained by taking the gradient of the disturbance potential ( $\phi$ ) to find the disturbance velocity and then adding the undisturbed velocity ( $\underline{q}(\underline{x}, t) = \underline{q}_o(\underline{x}, t) - \underline{q}_F(\underline{x}, t) + \nabla\phi(\underline{x}, t)$ ). Equation (4.83) is non-linear in the sense that the normal component of the undisturbed velocity on the actual body surface ( $(\underline{q}_o - \underline{q}_F) \cdot \underline{n}$ ) is included (geometric non-linearity), and the jump in the disturbance potential on the shed-vortex sheet ( $\Delta\phi_v$ ) and the sheet position ( $\underline{x}_v(t)$ ) depend on the disturbance potential ( $\phi(\underline{x}_o, t)$ ) distribution on the body surface (solution non-linearity and memory effect).

In practice the integral equation (4.83) can rarely be solved analytically, thus an appropriate numerical evaluation of the integral and an appropriate representation of the body surface and the wake sheet are required. One possible approach is that a panel-method approximation is used just as in the steady flow case and a suitable model is employed to represent the wake sheet. Then the boundary value problem is solved at discrete time steps with a small time increment during which the quantities of interest are assumed to be constant in time.

#### 4.6.7 Vortex model of shed wake sheet: Typical example

To include the influence of the shed-vortex sheet, the singularity strengths and the sheet geometry should be known. Among various computational schemes, the series of vortices can be used to represent the sheet geometry and to evaluate the equivalent potential on the body surface induced by a doublet distribution (potential jump across the sheet) on the shed vortex sheet. Giesing (1968a)<sup>13</sup> presented comparisons of the calculated location of the vortex sheet with photographs by Bratt (1953).<sup>14</sup>

<sup>13</sup>Giesing, J. P. (1968a), "Nonlinear Two-Dimensional Unsteady Potential Flow with Lift," *Journal of Aircraft*, vol. 5, no 2, pp. 135–143.

<sup>14</sup>Bratt, J. B. (1953), "Flow Patterns in the Wake of an Oscillating Aerofoil," *Aeronautical Research Council, Reports and Memoranda*, no. 2773.

The comparisons show that this model for the shed-vortex sheet produces remarkably good predictions of sheet position. Thus it is reasonable to adopt a concentrated vortex model because our approach here is aimed at a satisfactory solution rather than a rigorous one. In order to include more precisely the wake influence in the near region of the T. E., a small straight-line element attached to the T. E. is introduced exceptionally, over which a potential jump (doublet strength) is linearly distributed.

The potential and the velocity induced by a linear variation of doublet distribution ( $\mu^{(k)} = \mu_o^{(k)} + \delta_o^{(k)}\lambda$  where  $\lambda$  is the projected coordinate onto  $Ox$ -axis, the mid-point being an origin as depicted in Figure 4.5 ) over the straight-line element are given by (with the same notation as in the previous sections),

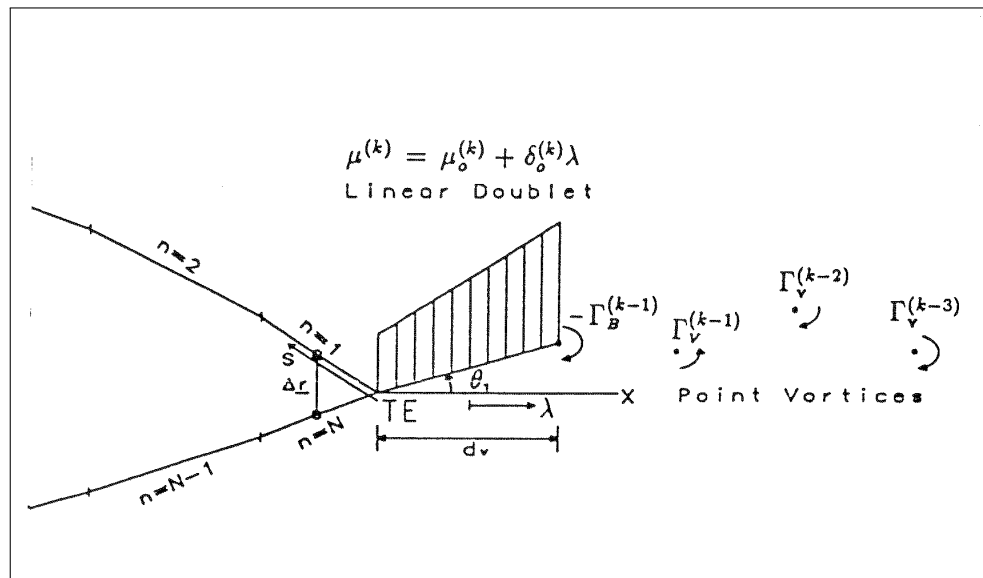


**Figure 4.5** A doublet straight-line element attached to the trailing edge and a series of concentrated vortices. The superscripts denote the time steps,  $(k)$  referring to the present time step.

The orientation of the element leaving the foil at the time of solution is unknown. For fixed values of the element length ( $\Delta v_1$ ) as an input parameter, the time increment ( $\Delta t^{(k)}$ ) between  $t^{(k)}$  and  $t^{(k-1)}$  and the inclination of the element to  $Ox$ -axis ( $\theta_1^{(k)}$ ) are to be determined as a part of the solution by an iteration procedure described in the next section. The vorticity on the straight-line wake

element attached to the T. E,  $(\gamma_{TE})$  is given by

$$\gamma_{TE}^{(k)} = \frac{\Gamma_B^{(k-1)} - \Gamma_B^{(k)}}{\Delta v_1} \quad (4.84)$$

where  $\Delta v_1 = \frac{d_v}{\cos \theta_1}$  as indicated in Figure 4.5 .

A downstream wake of concentrated vortices is formed from the vorticity shed at earlier times, which is assumed to be concentrated into discrete vortices whose strength is given by  $\Gamma_v^{(k)} = \gamma_{TE}^{(k)} \Delta v_1$ . These discrete vortices are convected with unchanged strengths from the previous position according to the (total) resultant velocities calculated at the center of each vortex at each successive time interval. The time increment  $\Delta t^{(k)}$  is calculated approximately by dividing by  $\Delta v_1$  the local total velocity at the mid-point of the straight-line wake element attached to the T. E.

The orientation of the straight-line element is determined such that it is parallel to the local resultant velocity at the mid-point of that element. This model is shown pictorially in Figure 4.5 .

Now the last integral of (4.83) leads equivalently to the potential induced by the series of concentrated vortices, which is written down as the sum of the potential induced by each concentrated vortex. This equivalent replacement demands a determination of reference value of the angle involved in the vortex-potential.

The reference orientation of each vortex potential is taken as a line parallel to the  $Ox$ -axis. The difference of phase does not affect directly the velocity and the time derivative because all values of  $\phi_j^{(k)}$  differs uniformly in the amount of the phase difference as an additive constant and the pure effect of the total vortex system becomes eventually the phase of the cut extending from the end of the wake sheet to far downstream which may initially be taken as zero. It is easily seen that the phase difference leads to the increment of constant values of  $\phi$  over the closed body surface, from the identity

$$\frac{1}{2\pi} \int_B \frac{\underline{n}(\underline{x}_v) \cdot (\underline{x} - \underline{x}_v)}{|\underline{x} - \underline{x}_v|^2} dl_x = 0, \quad (4.85)$$

for a point  $\underline{x}_v$  outside a closed body. It should be noticed that the contribution of the point vortex at the downstream end point of the doublet straight-line element (labelled ' $-\Gamma_B^{(k-1)}$ ', in Figure 4.5) should be included in the equivalent replacement of this concentrated vortex model.

As the number of point vortices shed increases with time steps, the computations for induction between them grow with the square of their number. To reduce the computation time, one can simply ignore the vortices beyond a given number or distance behind the T. E. (about 10 times of the chordlength), since their influence on the body decreases with distance. Another way is, although it is still an approximation, that the two of the oldest shedding vortices beyond a given number (say 250 herein) are amalgamated to reduce the number of point vortices (actually in a computer code it keeps the same number after this time step).

For this operation, two point vortices of strengths  $\Gamma_1$  and  $\Gamma_2$  at  $\underline{x}_1$  and  $\underline{x}_2$ , respectively, are replaced by one point vortex of strength  $\Gamma_1 + \Gamma_2$  at the position given by  $(\underline{x}_1|\Gamma_1| + \underline{x}_2|\Gamma_2|)/(|\Gamma_1| + |\Gamma_2|)$ . However in most calculations with moderately reasonable input parameters, it is better to avoid this amalgamation possibly because of lack of its physical equivalence.

#### 4.6.8 Solution procedures

The numerical solution procedures are similar to that in the steady panel method approximation except that there is an another contribution due to a series of concentrated vortices (equivalent to the potential jump (doublet distribution) on the geometrically time-varying vortex sheet). The solution for the unsteady flow about a body is calculated starting at  $t = 0$  and continuing the process at successive time steps.

The unsteadiness of the flow is assumed to start from the mean position for harmonic motions of a foil or with zero circulation for a sudden start-up problem.

At successive time steps a shed vortex is defined and is convected with the local mean velocity without change of its strength. Hence this will induce a

known potential back on the body and this effect must be included in the solution of the integral equation.

This approach is carried out as follows. At time  $t^{(k)}$ , the basic set of equations for  $N + 1$  unknowns ( $\phi_j^{(k)}, j = 1, \dots, N$  and  $\theta_1^{(k)}$ ) can be formulated. First the  $N$  algebraic equations associated with the integral equation (4.83) can be written down in a matrix form with unknowns  $\phi_j$  :

$$[A_{mj}] \left\{ \phi_j^{(k)} \right\} = \left\{ B_m^{(k)} \right\} + [C_{ml}^{(k)}] \{(\Gamma_v)_l\} + \left\{ D_m^{(k)} \right\}, \quad (4.86)$$

for  $m, j = 1, \dots, N$  &  $l = 1, \dots, (k - 1)$ ,

where  $[A_{mj}]$  is the coefficient matrix of the set of linear equation which approximates the integral equation and each of which represents the induced potential at the  $m$ -th control point due to the unit density doublet distribution on the  $j$ -th panel,  $\{B_m^{(k)}\}$ ,  $[C_{ml}^{(k)}]$ ,  $\{(\Gamma_v)_l\}$  and  $\{D_m^{(k)}\}$  represent the effect due to the equivalent source distribution with strength  $(\underline{q}_F - \underline{q}_O) \cdot \underline{n}$  on the body surface, the effect due to the series of concentrated vortices with strength  $\Gamma_v$  on the downstream wake and the effect due to the doublet distribution with a linear variation over the straight-line wake sheet element attached to the T. E. (with unknown  $\theta_1^{(k)}$ ), respectively.

Another condition to determine  $\theta_1^{(k)}$  is that the local resultant velocity at the mid-point of the straight-line wake sheet element attached to the T. E. is parallel to its orientation. This requires an iteration process together with an allowable tolerance, using the previously updated  $\phi_j^{(k)}$  and  $\Delta\phi_v|_{TE}$  to calculate the local resultant velocity.

The initially guessed values for starting this iterative process are taken as those obtained at the previous time step to reduce the iteration process time. Thus with these guessed values, the  $N$  linear equations are solved to obtain  $\phi_j^{(k)}, (j = 1, \dots, N)$ .

Once the temporary values of  $\phi_j^{(k)}$  are known during the iteration process,  $\Delta\phi_v|_{TE}$  and the local resultant velocity can be calculated, from which the newly updated value  $\theta_1^{(k)}$  is found. Such a procedure is repeated until  $\theta_1^{(k)}$  and  $\Delta\phi_v|_{TE}$  have converged within the desired allowance. This results in a relatively rapid

convergence, for example, requiring usually 2-5 iterations for convergence within 1 % change relative to the previously updated value for  $\Delta\phi_v|_{TE}$  and 0.1° change for  $\theta_1^{(k)}$ .

Once the final values after the iteration procedure have been determined, the tangential component of the disturbance velocity at the body surface is computed (in the moving frame). The disturbance tangential speed can be obtained by numerical differentiation of the surface potential in the local tangential direction at the actual surface point at which the constant value of  $\phi_j^{(k)}$  over the panel is assumed to be representative.

A piecewise constant representation of  $\phi$  must be fitted with a polynomial form over several nearby panels before being differentiated. Here for improvement of the numerical accuracy (especially near the L. E.) in the calculation of the disturbance surface speed ( $\nabla\phi \cdot \underline{t}$ ), the cubic spline (e.g., the B-spline or the tension cubic spline)<sup>15</sup> might be used for curve-fitting of the discrete values of the disturbance potential.

If the discrete values of  $\phi_j^{(k)}$  versus the angular parameter  $\varphi$  (that is the transformed variable used for ‘cosine-spacing’ previously) instead of the coordinate  $x$  were fitted, the disturbance surface speed is obtained by the chain rule;  $\frac{d\phi}{ds} = \frac{d\phi}{d\varphi} \cdot \frac{d\varphi}{ds}$ . The reason for the choice of the parametric spline with  $\varphi$  is that we can avoid fitting the rapid change of  $\phi$  near the L. E. and the T. E. from the use of the  $x$ -coordinate of the discrete points. Therefore the discrete values of  $\phi$  are fitted smoothly with higher-order accuracy when using a uniform spacing (i.e.,  $\Delta\varphi = 2\pi/N$ ) over the interval of the parameter ( $2\pi$ ).

Now the total tangential speeds are obtained by adding the tangential component of the undisturbed velocity ( $\underline{q}_o - \underline{q}_F$ ). In the unsteady pressure relation (4.74), the time derivative term  $\frac{\partial\phi}{\partial t}$  is approximated as

$$\frac{\partial\phi_j^{(k)}}{\partial t} = \frac{\phi_j^{(k)} - \phi_j^{(k-1)}}{t^{(k)} - t^{(k-1)}}. \quad (4.87)$$

<sup>15</sup>The tension cubic spline was suggested by McCartin, B. J. (1983), “Applications of Exponential Splines in Computational Fluid Dynamics,” *AIAA Journal*, vol. 21, no. 8, pp. 1059-1065. It is used to get rid of unwanted wiggles (extraneous inflection points), that might occur in some intervals when fitting the discrete values by the original cubic spline, by applying local tensions additionally to those intervals.

By direct integration of the pressure coefficient distribution, the force and moment coefficients are obtained. The integration is also performed after fitting the integrand of the integral expressions ((4.89) and (4.90)) for the forces and moment coefficients by integrating the fitting values by the spline. It is noted that the required slopes at the end points of the spline interval are estimated by parabolically fitting of three points—each end point and two neighboring points. Once the solution at time  $t^{(k)}$  has been determined, the model is set up for time  $t^{(k+1)}$  with the wake pattern as calculated from the solution at time  $t^{(k)}$ .

The distributed vorticity on the straight-line wake sheet element attached to the T. E. at time  $t^{(k)}$  is now assumed to be concentrated into a vortex of strength  $\gamma_{TE}^{(k)} \Delta v_1$  at time  $t^{(k+1)}$  situated at the next moving point convected with the local mean velocity at the mid-point of the wake element. The resultant velocity at the center of each of the other concentrated vortices in the wake is calculated from the solution at time  $t^{(k)}$  and then the position of that vortex at time  $t^{(k+1)}$  follows directly.

Especially for a 2-D foil, the force components in the  $x$ - and  $y$ -direction, of the moving frame and the moment about  $\underline{x}_m$  (positive is taken as counterclockwise) acting on the foil are given by, respectively,

$$F_x \underline{i} + F_y \underline{j} = - \oint_B C_p(\underline{x}, t) \underline{n} dl_x, \quad (4.88)$$

and

$$C_M \underline{k} = - \oint_B (\underline{x} - \underline{x}_m) \times C_p(\underline{x}, t) \underline{n} dl_x. \quad (4.89)$$

These are non-dimensionalized by the chordlength  $c$ , the fluid density  $\rho$  and the reference speed ( $U_o$ ) with a factor 1/2.  $F_x$  and  $F_y$  are the force components in  $x$ - and  $y$ -direction, respectively, in the moving frame (see Figure 4.6). Lift and drag coefficients are resolved relative to an orientation usually specified in the inertial frame at a given instant:

$$C_L = F_y \cos \alpha(t) - F_x \sin \alpha(t), \quad (4.90)$$

$$C_D = F_x \cos \alpha(t) + F_y \sin \alpha(t), \quad (4.91)$$

where  $\alpha(t)$  is an angle of attack at an instantaneous time.

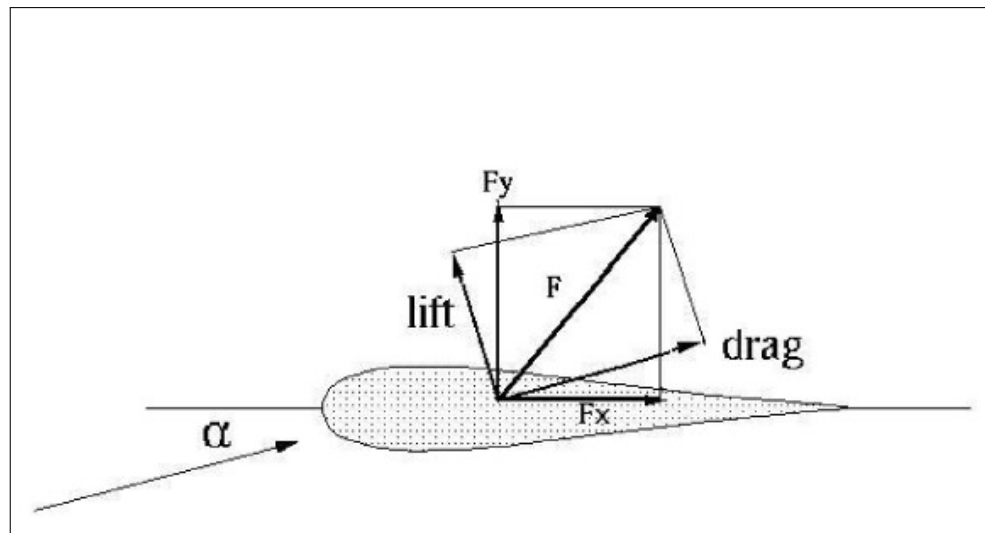


**Figure 4.6** Force diagram of 2-D foil.

Each individual step of the numerical solution process is outlined as follows:

- (1) Read the body geometry, the mean angle of attack, the type of unsteady motions and/or flows. For application of the combined flow situation, the motions and/or flows are decomposed into harmonic components specified by amplitude, frequency and phase of each component. Also the number of discretized panels on the body surface, the number of the time steps to be performed and the length of the straight-line wake sheet element attached to the T. E. are input parameters.
- (2) Discretize the body surface by 'cosine-spacing' to generate the panel geometry and each geometrical parameter such as control point, (approximate) representative surface point and tangential vector.
- (3) Calculate the influence coefficients at the control points induced by the flat panels representing the body surface.
- (4) Calculate the results of the steady flow case at the mean position or at an ultimate time which will be used as the initial starting value or for normalization.

- (5) Guess initially at the  $(k)$ -th time step the orientation of the wake sheet element, the shed vorticity at the T. E. and the potential jump at the T. E. by assigning those values computed at the previous time step.
- (6) Calculate the undisturbed velocity specified by the unsteady motion and/or the flows observed in the moving frame, from which the no-penetration condition is imposed at each control point.
- (7) Calculate the right-hand side of the matrix system of the linear algebraic equations, including the effect of the concentrated vortex system newly updated in position from the previous time step.
- (8) Solve the  $N \times N$  matrix system of linear equations for the  $N$  unknowns  $\phi_j^{(k)} (j = 1, 2, \dots, N)$  by using the inversion by the decomposition of the matrix.
- (9) Compute the orientation of the straight-line wake sheet element, the shed vorticity strength and its associated potential jump at the T. E.
- (10) Repeat steps (6) through (9) until the converged values of the above quantities are obtained within a given allowance or until a prescribed allowable number of iteration are processed.
- (11) Calculate the convective velocities at the vortex cores at the present time step to update their positions for process at the next step. An amalgamation of two distant vortices is carried out at this stage if desired.
- (12) Find the surface speed and pressure distribution, the force components and the moment about a given point, by using the exponential spline to differentiate the values of the surface potential and to evaluate the associated integrals.
- (13) Repeat steps (5) through (12) until a given or enough number of time steps are executed to achieve the steady-state solution or to carry the solution far downstream.

#### 4.6.9 Numerical results: Steady flow cases

Numerical and analytical surface (disturbance) potentials on an ellipse of 10% thickness-chord ratio at  $10^\circ$  angle of attack in steady uniform ( $K = 0$ ) and shear ( $K = 1$ ) onset flow are compared in Figure 4.7. The total surface speeds in the same flow situation are also compared in Figure 4.8.

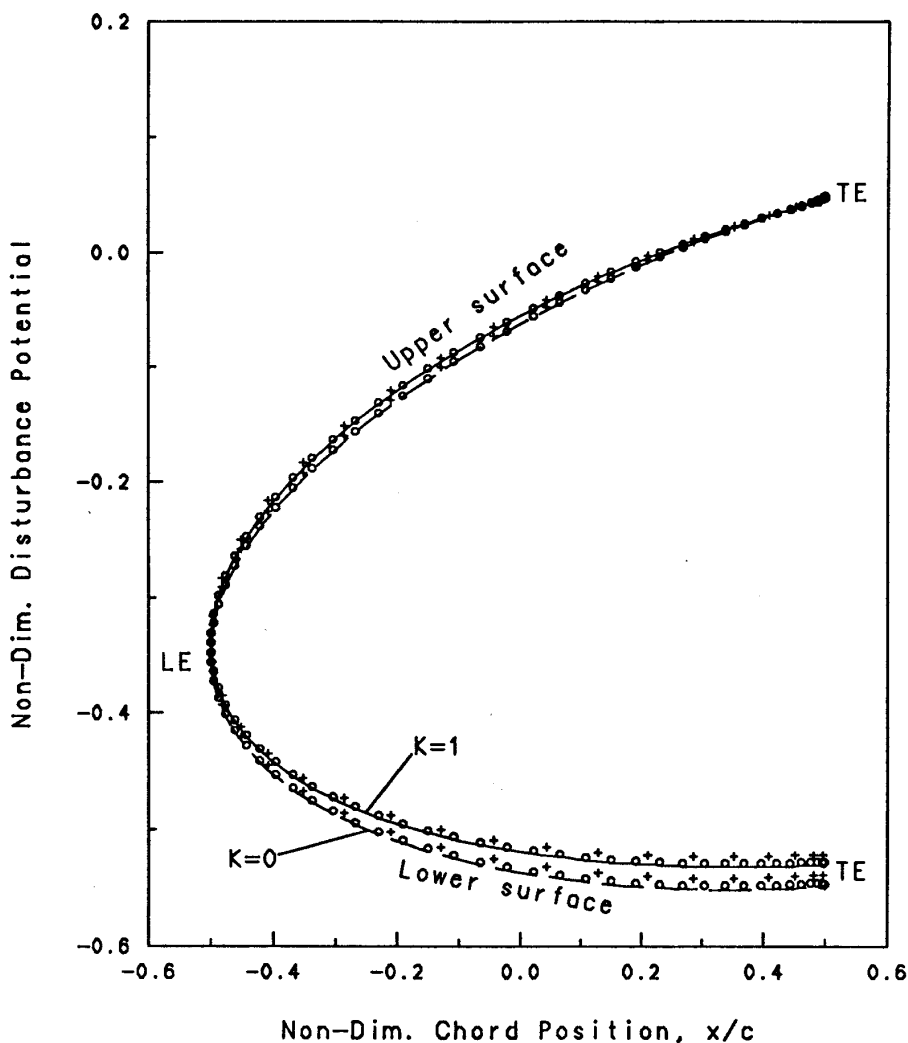


**Figure 4.7** Comparison of numerical and analytical disturbance potentials on the surface of an ellipse ( $\tau = 10\%$ ) in steady uniform ( $K = 0$ ) and shear ( $K = 1$ ) flow (at  $\alpha = 10^\circ$ ). The broken and the solid lines denote the analytical results for  $K=0$  and for  $K=1$ , respectively. The symbols denote the numerical results, using two different number of panels (+,  $N = 36$ ; o,  $N = 72$ ).

For the convergence check of the numerical model, two different number of panels ( $N = 36, 72$ ) have been chosen. Good convergence of the solution is

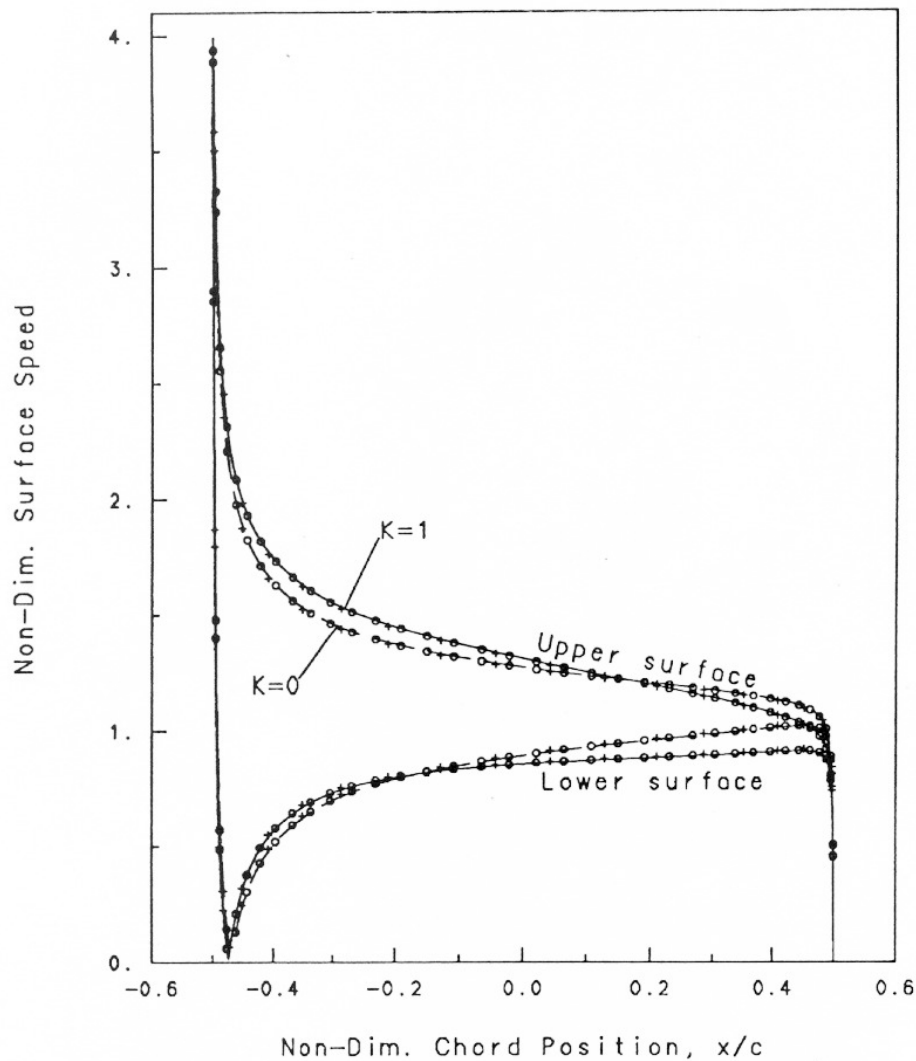


**Figure 4.8** Comparison of numerical and analytical total surface speeds on the surface of an ellipse in steady uniform and shear flow. Legends are the same as those in Figure 4.7 .

observed over the entire foil surface. It is seen that the numerical results are locally in good agreement with the analytical ones obtained by the conformal transformation, even when using a moderate number of straight-line elements for representation of foil geometry.

Figure 4.7 shows that the circulation ( $\Delta\phi|_{TE}$ ) for the case  $K = 1$  is less than that of the case  $K = 0$ . Increased speed on the upper surface in the case of  $K = 1$  tends to stimulate the flow downstream toward to the T. E. so as to satisfy the Kutta condition with the reduced value of  $\Gamma_B$  than that in the uniform flow case.

Figure 4.8 shows a difference in shape of the surface speed distribution between the uniform and shear flow cases. This figure compares velocities rather than pressure coefficients to look directly at the shear-flow effect on velocity distribution and to avoid uncertainty about the reference pressure for shear-flow case. The velocity curve of the shear flow case ( $K = 1$ ) seems to be obtained by rotating that of the uniform flow case ( $K = 0$ ) in the rotational direction of the shear flow.

In Figure 4.9, numerical and analytical lift and moment (about the mid-chord) coefficients versus angle of attack for various velocity gradient values ( $K$ ) are compared for a Moriya foil ( $\epsilon = 0.05, \delta = 0.1$ ) whose profile shape is symmetric conventional with thickness-chord ratio of 10 % (see Moriya (1941) or Suh (1990) for details). It is seen that the numerical results agree well with the analytical ones, which expected since there is good agreement of surface speed as shown in Figure 4.8. The results indicate that lift coefficient is fairly linearly proportional to angle of attack over its moderate range.

#### 4.6.10 Numerical results: Unsteady flow cases

##### 4.6.10.1 Start-up problems

There are two non-linear aspects to be considered when employing numerical methods for combined flow situations proposed herein— finite thickness of a foil and distortion of the wake sheet (both of which have been neglected in

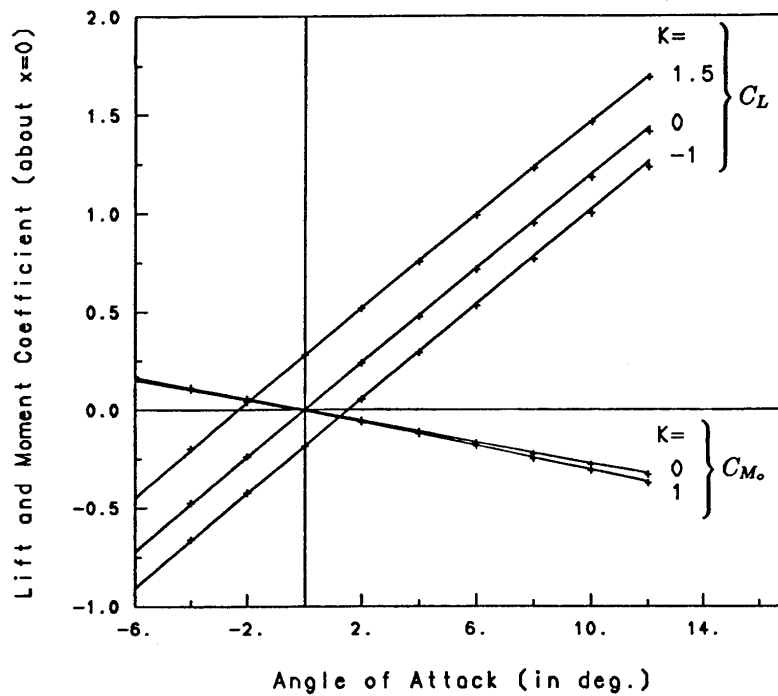


**Figure 4.9** Comparison of numerical and analytical lift and moment coefficients (about the mid-chord point) versus angle of attack for a Moriya (1941) foil ( $\epsilon = 0.05$ ,  $\delta = 0.1$ ) in steady shear flow. —, analytical; +, numerical.

the derivation of the classical linear analytical solutions). Figure 4.10 shows, with varying thickness of a foil, numerical lift growths for start-up problems of NACA 4-digits foil sections,<sup>16</sup> together with the linearized analytic solution (i.e., Wagner function,  $W(\sigma)$ ). These test cases have been chosen to emphasize the non-linear aspects. The effect of foil thickness on growth of lift seems to be more significant quantitatively than that of the angle of attack from the viewpoint of realistic flow situations.

To see the distorted shedding vortex sheet, Figure 4.11 shows the calculated positions of vortex cores for an NACA0012 foil at  $\alpha = 10^\circ$ . It is seen that the roll-up behavior occurs together with stretching near the end of the vortex sheet.

<sup>16</sup>To generate closed round shape at the T. E. instead of originally defined blunt shape (Abbott & Doenhoff (1959), p. 113), we have used a modified thickness distribution near the T. E. with a parabola of the form specified by matching the conditions of the offset and slope at  $x = 0.492404$ :  $Y_t/t_o = \pm\sqrt{0.5 - x} (0.231902 - 1.316268(0.5 - x))$ ,  $x > 0.492404$ .

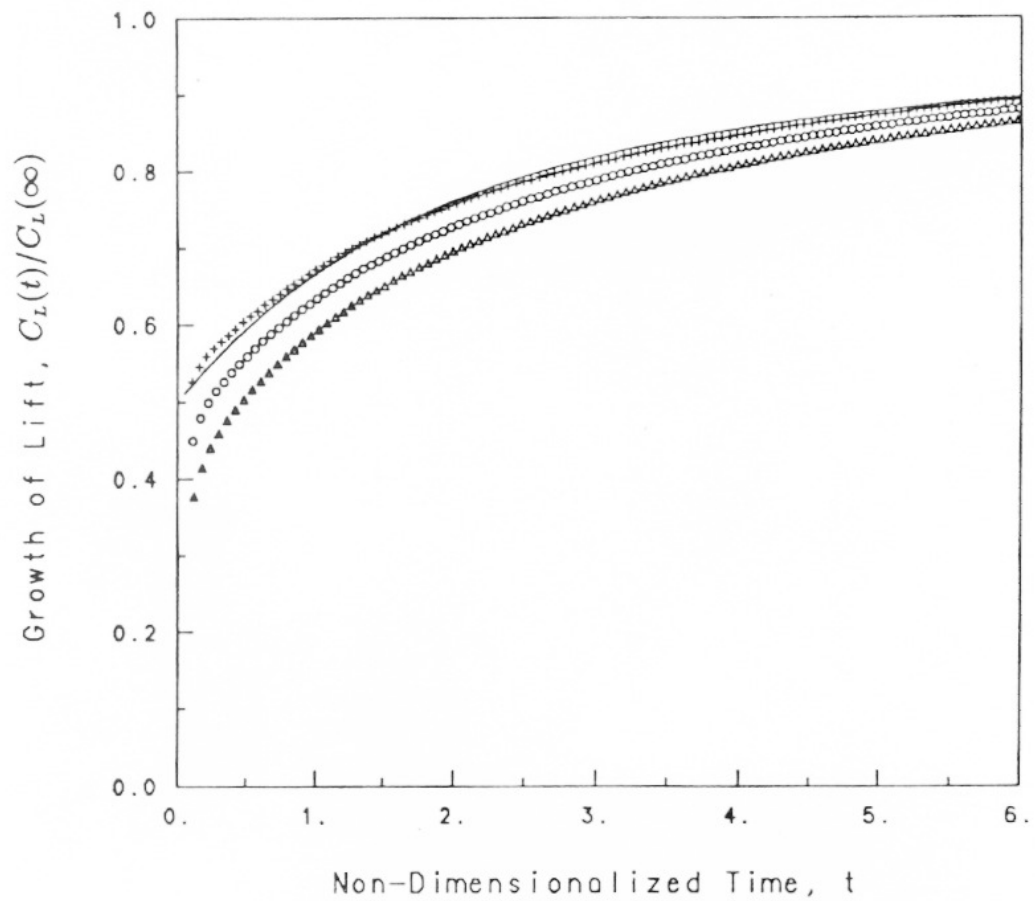


**Figure 4.10** Growth of lift for sudden start-up of NACA0006, NACA0012 and NACA 0018 foils in uniform onset flow (at  $\alpha = 10^\circ$ ). The solid line denotes the linearized analytical solution for a flat plate (Wagner (1925)). The symbols denote the present numerical results with  $N = 36$ ,  $\Delta v_1 = 0.05$  (+, NACA0006; o, NACA0012; Δ, NACA0018).

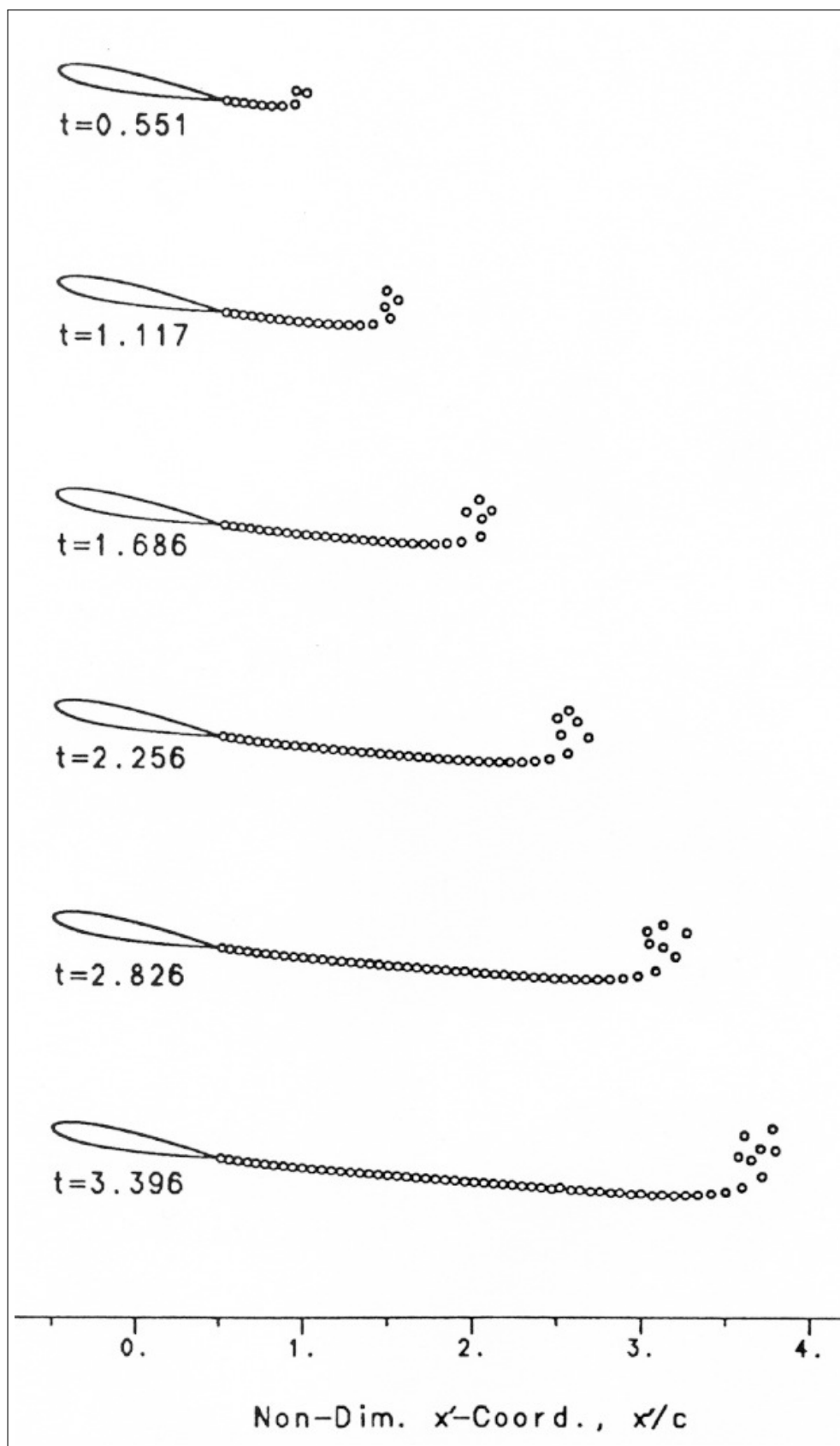


**Figure 4.11** Calculated location of vortex cores for start-up of an NACA0012 foil at  $\alpha = 10^\circ$  with  $\Delta v_1 = 0.05$ . The non-dimensionalized time  $t$ 's correspond to the time steps ( $k$ ) = 10, 20, 30, 40, 50, 60.

#### 4.6.10.2 Harmonic heave motion

Figure 4.12 presents the calculated location of the vortex cores representing the shed-vortex sheet for harmonic heave motion (with a reduced frequency  $k = 2.15$  and a heave amplitude  $h_o = 0.018$ ) of an NACA0015 foil in uniform flow. It shows that the numerical model for calculation of position of the sheet predicts a shape similar to that calculated by Giesing (1968a) and similar to that observed by Bratt (1953). Therefore this distortion of wake sheet shape may affect significantly on the flow characteristics of an interference problem (like that between two moving foils).

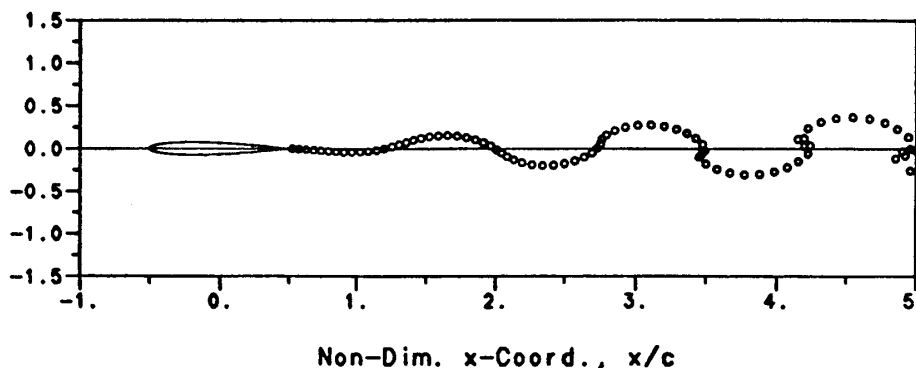


**Figure 4.12** Calculated location of vortex cores for harmonic heave motion of an NACA0015 foil in uniform flow (for  $\alpha = 0^\circ$ ,  $k = 2.15$ ,  $h_o = 0.018$ ).

With varying thickness of an NACA 4-digits foil section, time variation of lift coefficient and its fluctuation magnitude for various reduced frequencies  $k$  for heave motion are shown in Figure 4.13. For a comparison purpose, the linearized analytical solution is also presented:<sup>17</sup>

$$C_L(t) = -4\pi h_o k [Re(C(k)) \cos(2kt + \varphi) - \{Im(C(k)) + 0.5k\} \sin(2kt + \varphi)] \quad (4.92)$$

where  $C(k)$  is the Theodorsen function,  $h_o$  is an amplitude of heave motion and  $\varphi$  is a phase of heave motion. The magnitude of fluctuating lift decreases with increasing thickness of a foil. This thickness effect becomes larger as  $k$  increases, but a relative difference is mostly the same over a wide range of  $k$ .

<sup>17</sup>Küssner (1960), Hewson-Browne (1963), and van de Vooren & van de Vel (1964) have addressed second-order corrections by considering the separate influence of finite foil thickness at zero mean angle of attack.

For the case of an NACA0012 foil, there is about 7% change of the magnitude of fluctuating lift relative to the magnitude for an NACA0006 foil.

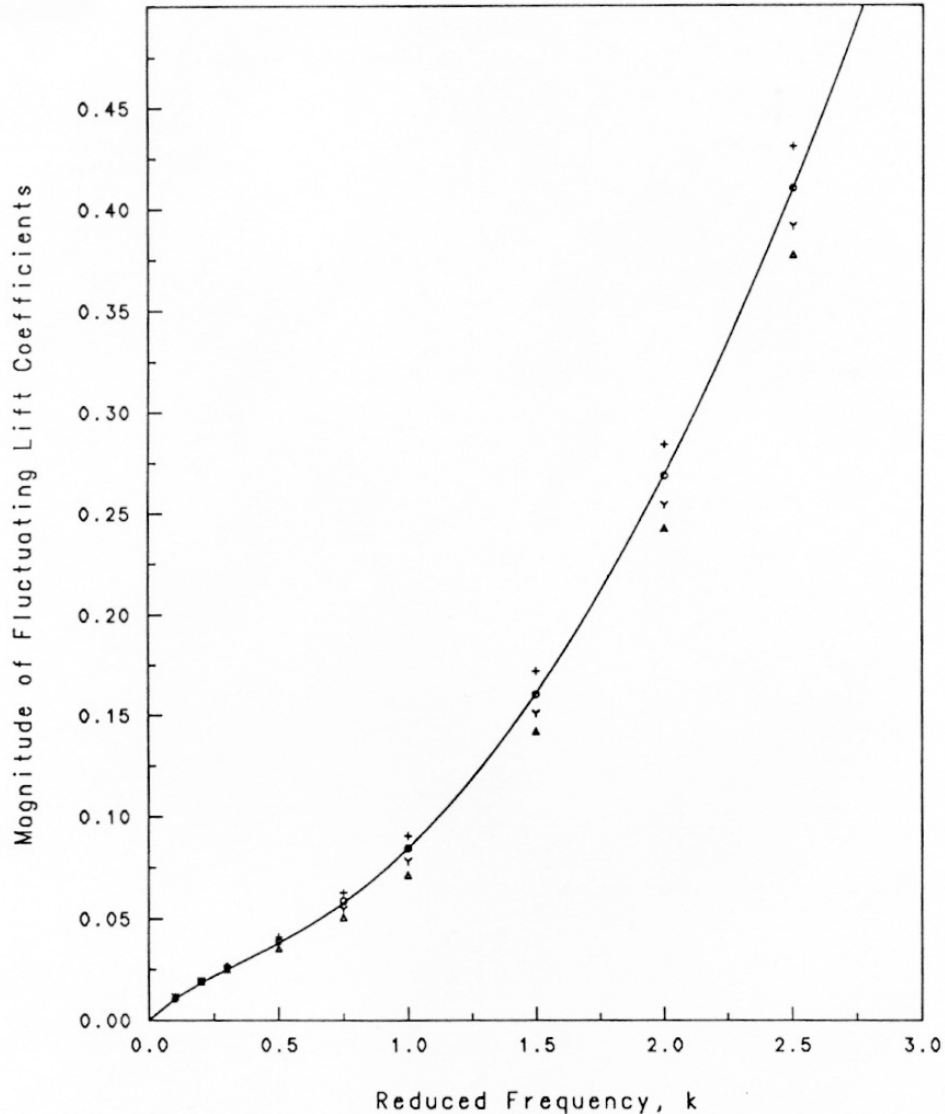


**Figure 4.13** Magnitude of fluctuating lift with various reduced frequencies for heave motion of NACA0006, NACA0012, NACA0018 and NACA0024 foils in uniform flow ( $K = 0$ ) (for  $\alpha = 0^\circ$ ,  $h_o = 0.01$ ). +, NACA0006; o, NACA0012; Y, NACA0018 Δ, NACA0024. The solid line denotes the linearized analytical solution (Theodorsen (1935)).

#### 4.6.10.3 Concluding remarks on combined motions

Although not presented herein, the present numerical algorithm can be extensive to arbitrary combined flow situations that is usually composed of heave,

pitch motions and vertical gusts. This combined flow situation can be modeled as that of a foil moving with a forward speed and undergoing the assumed periodic motion in uniform onset flow and the vertical gust. The lift coefficient obtained by superposition of each classical linearized analytic solution plus the numerical steady value at the mean flow condition (i.e.,  $\alpha_m = 0^\circ$ ) is available. The superposed linearized solution gives fairly good agreement in trend of the overall forces with the non-linear numerical results.

This flow situation may be considered as that about the blade section of a marine propeller, for which there is a large multiple blade-order frequency component of non-uniformity in ship wake flow. Therefore a superposition (of multiple gusts) of fluctuating lift coefficient (which has been used in many practical propeller problems) might be appropriate in combined flow case.

## 4.7 Formulation in Three-dimensions

### 4.7.1 Extension to 3-D wing

Like 2-D foils, Figure 4.14 represents a relative configuration of a wing in the inertial and moving frames with appropriate notations to be used for the formulation of the boundary value problem. The coordinate system is the same as the 2-D system, but we add the  $z$ -axis in third (vertical) direction.

Recall that the continuity equation for the disturbance velocity reduces to  $\nabla \cdot \underline{u}$ . The present concern is one whether the disturbance velocity is irrotational in the moving frame when the total velocity is irrotational and then the present procedure for solving the potential flow can be applied extensively. The vorticity of the inherent irrotational flow can be expressed by, in the inertial frame,

$$0 = \nabla' \times \underline{q}'_T = \nabla' \times (\underline{q}_F + \underline{q}) = 2 \underline{\Omega} + \nabla \times \underline{q}, \quad (4.93)$$

or

$$\nabla \times \underline{q} = -2 \underline{\Omega} \quad (4.94)$$

This indicates that the vorticity of a flow in the non-inertial (moving) reference

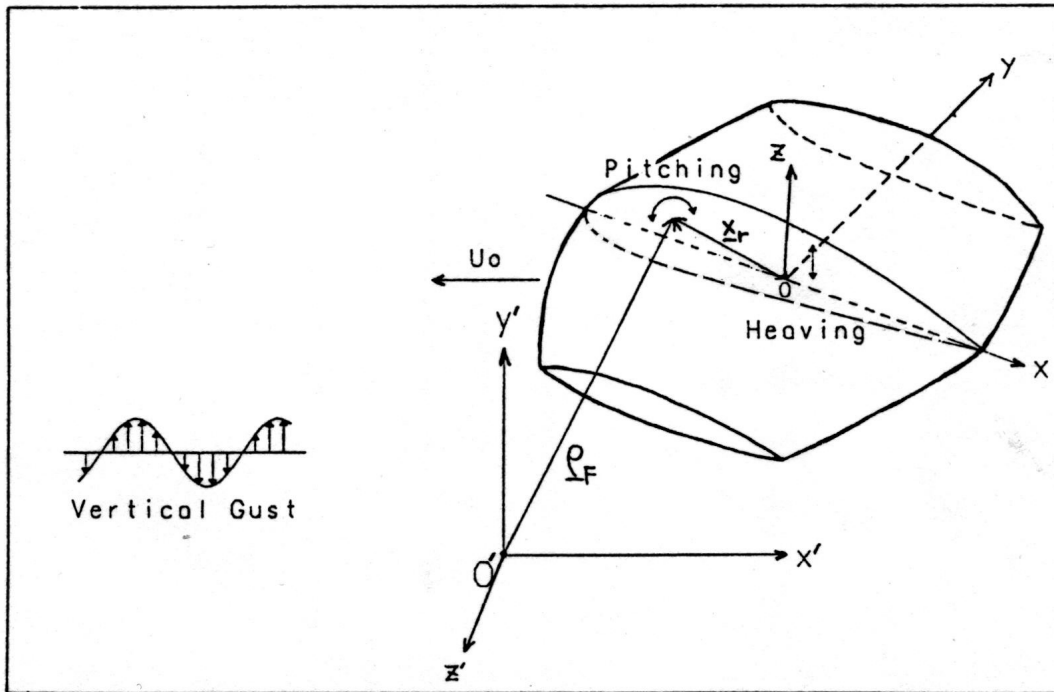


**Figure 4.14** The coordinate systems and a combined unsteady flow situation for a 3-D wing.

frame is different from that of a flow in the inertial frame.

However, let us express  $\underline{q}$  in terms of the disturbance caused by a body, then the expression reduces to

$$\nabla \times \underline{q} = \nabla \times (\underline{q}_o - \underline{q}_F + \underline{u}) = -2\underline{\Omega} + \nabla \times \underline{u} \quad (4.95)$$

From Eqs. (4.94) and (4.95),  $\nabla \times \underline{u} = 0$  must be satisfied which means that the disturbance velocity field measured in the moving frame is also irrotational. Hence we can introduce a disturbance velocity potential ( $\underline{u} = \nabla\phi$ ) which is governed by the Laplace equation:

$$\nabla^2\phi = 0 \quad (4.96)$$

The computational procedures for solving a related problem are similar to those for 2-D foil.

### 4.7.2 Velocity components at a panel surface

Suppose that the velocity components in direction of two non-orthogonal coordinates  $(s_1, s_2)$  on a panel surface have been computed.

$$v_1 = \frac{\partial \phi}{\partial s_1}, \quad v_s = \frac{\partial \phi}{\partial s_2} \quad (4.97)$$

Now we should know the orthogonal velocity components from these non-

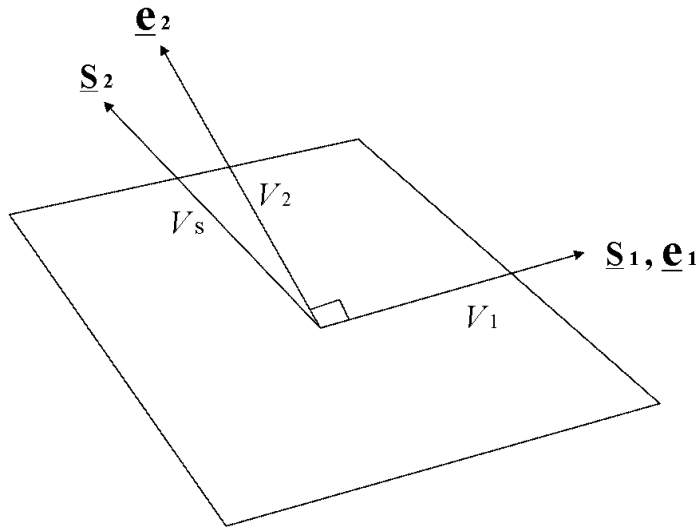


**Figure 4.15** Velocity component calculation for local non-orthogonal coordinates of panel surface.

orthogonal components. Take an orthogonal coordinate system  $(e_1, e_2)$  where  $e_1 = s_1$  with the corresponding unit vectors. (See Figure 4.15 ). Then

$$\begin{aligned} v_s \underline{s}_2 &= v_1 \underline{e}_1 + v_2 \underline{e}_2 \\ v_s \underline{s}_2 \cdot \underline{s}_2 &= v_1 (\underline{e}_1 \cdot \underline{s}_2) + v_2 (\underline{e}_2 \cdot \underline{s}_2) \\ v_2 &= \frac{v_s - v_1 (\underline{e}_1 \cdot \underline{s}_2)}{(\underline{e}_2 \cdot \underline{s}_2)} \end{aligned} \quad (4.98)$$

### 4.7.3 Non-lifting flow about an ellipsoid

The analytic solution of the disturbance potential about an ellipsoid at zero angle of attack are given in Milne-Thomson (1968).<sup>18</sup> By superposing the analytic solutions at zero angle of attack relative to the different axes, we obtain the analytic solution for an oblique onset flow  $\underline{q}_0 = (U, V, W)$ . Then the surface speeds are found by differentiating the potential along the surface. For an ellipsoid whose geometry is specified as  $(x/a)^2 + (y/b)^2 + (z/c)^2 = 1$  where  $a, b, c$  are the length of the semi-axes, respectively, the surface speed  $\underline{q}_s$  is given by

$$\underline{q}_s = \left( \frac{x^2}{a^4} + \frac{y^2}{b^4} + \frac{z^2}{c^4} \right)^{-1} \cdot \left[ U \left( 1 + \frac{\alpha_0}{2 - \alpha_0} \right) \left\{ \left( \frac{y^2}{b^4} + \frac{z^2}{c^4} \right) \underline{i} - \frac{xy}{a^2 b^2} \underline{j} - \frac{zx}{c^2 a^2} \underline{k} \right\} + V \left( 1 + \frac{\beta_0}{2 - \beta_0} \right) \left\{ \left( \frac{z^2}{c^4} + \frac{x^2}{a^4} \right) \underline{j} - \frac{yz}{b^2 c^2} \underline{k} - \frac{xy}{a^2 b^2} \underline{i} \right\} + W \left( 1 + \frac{\gamma_0}{2 - \gamma_0} \right) \left\{ \left( \frac{x^2}{a^4} + \frac{y^2}{b^4} \right) \underline{k} - \frac{zx}{c^2 a^2} \underline{i} - \frac{yz}{b^2 c^2} \underline{j} \right\} \right] \quad (4.99)$$

where

$$\begin{aligned} \alpha_0 &= abc \int_0^\infty (a^2 + \lambda)^{-3/2} (b^2 + \lambda)^{-1/2} (c^2 + \lambda)^{-1/2} d\lambda \\ \beta_0 &= abc \int_0^\infty (b^2 + \lambda)^{-3/2} (c^2 + \lambda)^{-1/2} (a^2 + \lambda)^{-1/2} d\lambda \\ \gamma_0 &= abc \int_0^\infty (c^2 + \lambda)^{-3/2} (a^2 + \lambda)^{-1/2} (b^2 + \lambda)^{-1/2} d\lambda \end{aligned} \quad (4.100)$$

Figure 4.16 shows the chordwise distributions of the surface speed of an ellipsoid in an oblique onset flow. The numerical results at the three different spanwise positions have good agreement with the analytic solutions. Some discrepancy is observed near the leading edge and the trailing edge where the numerical resolution does not fairly follow the rapid change in the potential. In the numerical calculation, the bilinear distribution over each quadrilateral panel

<sup>18</sup>See, for details, Suh, J.-C., Lee, J.-T. and Suh, S.-B. (1992), "A bilinear source and doublet distribution over a planar panel and its application to surface panel methods," *Proc. 19th Symp. Naval Hydro.*, pp. 102–112.

was used to specify the singularity distribution on the surface. No-penetration condition (kinematic boundary condition) was applied at the *nodes of the panels* as the collocation points in the potential-based panel method. The resulting linear system of equations forms for the unknown nodal values of the disturbance potential. The surface speeds are calculated numerically using a second order fitting of the potential.

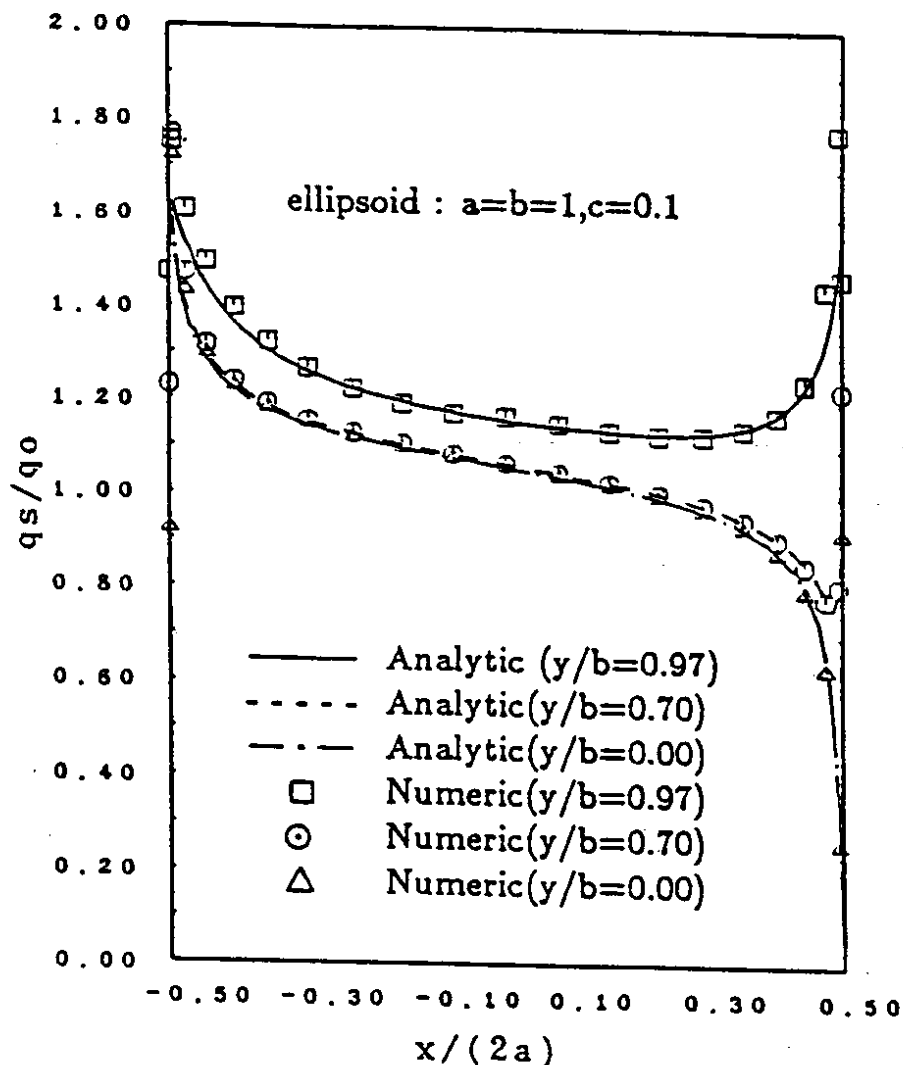


**Figure 4.16** The surface speed of an ellipsoid  $a = b = 1, c = 0.1$  in an oblique onset flow by using the quadrilateral panels with the bilinear singularity distribution. The onset flow velocity  $\underline{q}_0 = (1, 0, 0.1736)$ ; The number of chordwise and spanwise panels:  $N \times M = 40 \times 40$ .

#### 4.7.4 Lifting flow about a circular wing

In numerical implementation of the potential-based panel method for solving the potential flow around the lifting body, the trailing wake sheet is represented approximately as the doublet distribution of potential jump. One possible way to include the effect of the local variation of these doublet strengths is to use a bilinear distribution over each wake panel which is uniquely determined from imposed potential jump values at its four vertices.

The use of the bilinear distribution over the quadrilateral panels eliminates the discontinuity problem of singularity that is associated with the piecewise constant distribution. Then the singularity strength will be chosen to vary bilinearly across the panel. Therefore it is necessary to derive explicit and elegant closed forms of the induced potential and velocity due to the bilinear distribution. The closed forms are much computer-oriented and explicit so that we can obtain, with easier implementation, the matrix element of the linear system of algebraic equations in application of the surface panel methods. Chapter 5 presents the closed forms for computing the induced potential and velocity due to the bilinear distribution of source and/or doublet singularities over a planar panel.<sup>19</sup> The bilinear distribution cases includes, of course, both the constant and/or the linear distribution cases.

We calculated the circulation distribution for a circular wing, for which the linearized analytic solutions are available.<sup>20</sup> Numerical and analytical circulation distributions for a circular wing with NACA 4-digits section at  $5^\circ$  angle of attack are compared in Figure 4.17. For the implementation of the Kutta condition described previously, the constant singularity density was used for wing panels and the bilinear distribution for the trailing wake sheet elements extending on the  $xy$ -plane.

It is seen that the numerical method gives fair values compared to the linearized analytic solution using the moderate number of panels. Particularly the numerical results are in good agreement with the analytic ones near the tip

---

<sup>19</sup>See also Suh, J.-C., Lee, J.-T. and Suh, S.-B. (1992), "A bilinear source and doublet distribution over a planar panel and its application to surface panel methods," *Proc. 19th Symp. Naval Hydro.*, pp. 102–112.

<sup>20</sup>See Jordan, P. F. (1972), "Exact solutions for lifting surfaces," *AFOSR Scientific Report*, AFOSR-TR-72-1737.

where the circulation changes rapidly. The bilinear representation of the wake sheet singularity in the numerical method would be appropriate to include this local variation. Figure 4.17 shows that the circulation decreases as the thickness chord ratio increases. This feature is also found in the results provided by Lee, J.-T. (1987).

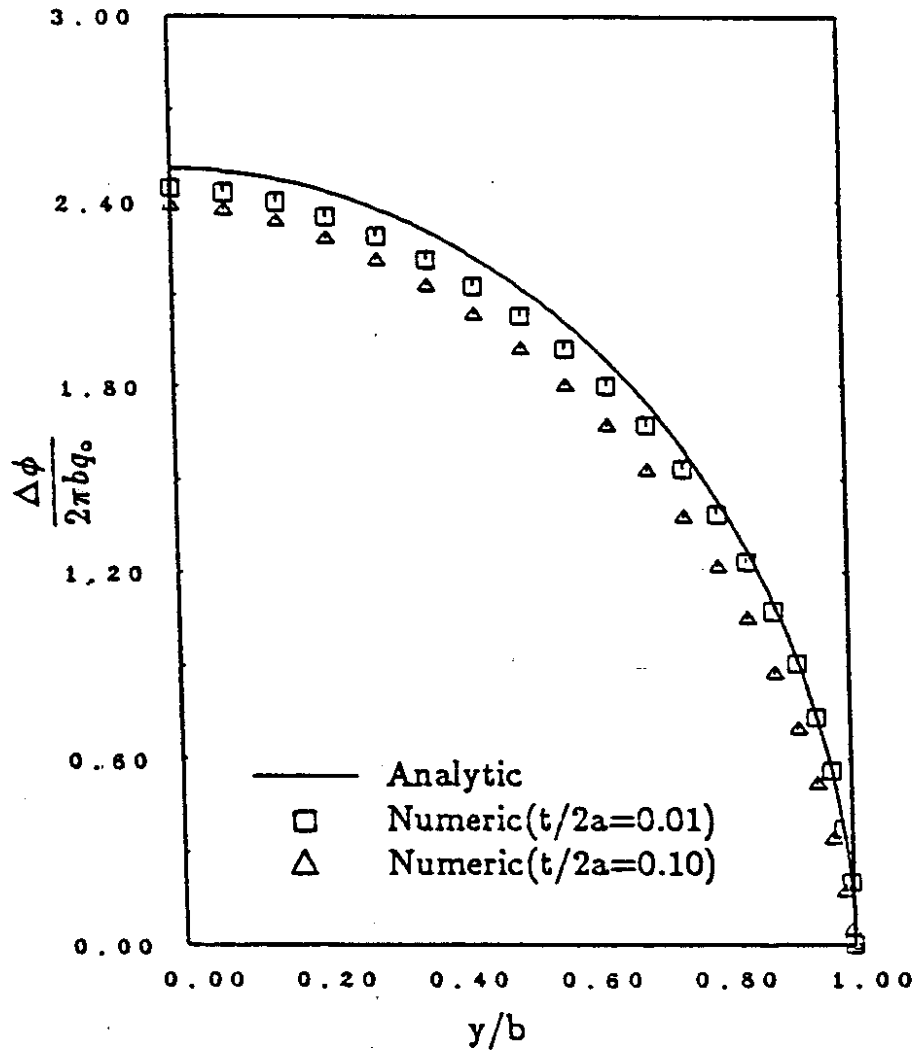


**Figure 4.17** Circulation distribution of a circular wing at  $\alpha = 5^\circ$  angle of attack. The number of chordwise and spanwise panels:  $N \times M = 40 \times 40$ .